Global bifurcations of the Lorenz manifold

Eusebius J. Doedel

Department of Computer Science, Concordia University, 1455 Boulevard de Maisonneuve O., Montréal, Québec H3G 1M8, Canada

Bernd Krauskopf and Hinke M. Osinga

Bristol Centre for Appled Nonlinear Mathematics, Department of Engineering Mathematics, University of Bristol, Bristol BS8 1TR, United Kingdom

Preprint of August 2006

(NOTE: image quality is reduced to restrict file size)

Abstract. In this paper we consider the interaction of the Lorenz manifold — the two-dimensional stable manifold of the origin of the Lorenz equations — with the two-dimensional unstable manifolds of the secondary equilibria or bifurcating periodic orbits of saddle type. We compute these manifolds for varying values of the parameter ϱ in the Lorenz equations, which corresponds to the transition from simple to chaotic dynamics with the classic Lorenz butterfly attractor at $\varrho = 28$.

Furthermore, we find and continue in ϱ the first 512 generic heteroclinic orbits that are given as the intersection curves of these two-dimensional manifolds. The branch of each heteroclinic orbit emerges from the well-known first codimension-one homoclinic explosion point at $\varrho = 13.9265$, has a fold and then ends at another homoclinic explosion point with a specific ϱ-value. We describe the combinatorical structure of which heteroclinic orbit ends at which homoclinic explosion point. This is verified with our data for the 512 branches from which we automatically extract (by means of a small computer program) the relevant symbolic information.

Our results on the manifold structure are complementary to previous work on the symbolic dynamics of periodic orbits in the Lorenz attractor. We point out the connections and discuss directions for future research.

AMS classification scheme numbers: 34C37, 70K44, 37Gxx

1. Introduction

We consider the well-known Lorenz equations [24], which can be written as the vector field in $\mathbb{R}^3$ given by

$$\begin{cases} \dot{x} &= \sigma(y-x), \\ \dot{y} &= \varrho x - y - xz, \\ \dot{z} &= xy - \beta z. \end{cases} \tag{1}$$

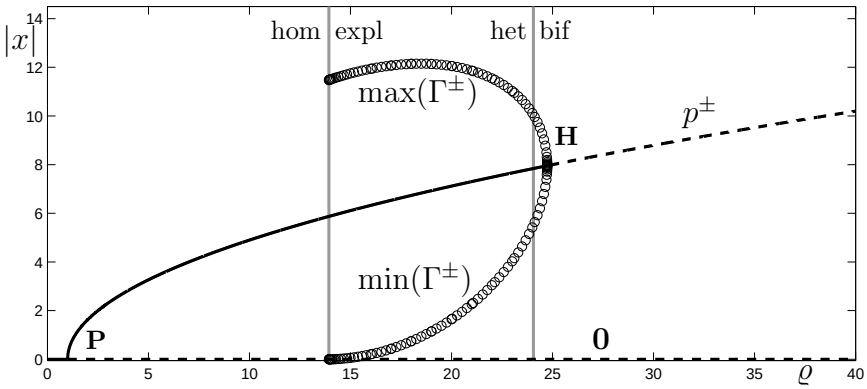

Figure 1. Bifurcation diagram of the equilibria and (saddle) periodic orbits of (1) as a function of ϱ. Indicated are the pitchfork bifurcation **P** of the origin at $\varrho = 1$, the homoclinic explosion point at $\varrho_{\mathtt{r}} \approx 13.9265$, the heteroclinic bifurcation at $\varrho_{\rm het} \approx 24.0579$ where there is a pair of heteroclinic orbits from **0** to $\Gamma^{\pm}$, and the subcritical Hopf bifurcation **H** of the secondary equilibria at $\varrho_H = \frac{470}{19} \approx 24.7368$.

Equations (1) were derived by E.N. Lorenz in the 1960s as a much simplified model of convection dynamics in the atmosphere and, quite by accident, he found that they display very sensitive dependence on the initial condition. Indeed for the now classic parameters values of $\sigma = 10$, $\beta = 8/3$, and $\varrho = 28$ one finds the butterfly-shaped Lorenz attractor, which has since emerged as arguably the most famous example of a chaotic attractor. An important and well-known feature of the Lorenz attractor and the Lorenz equations (1) is their symmetry

$$(x, y, z) \mapsto (-x, -y, z)$$

of rotation by π about the z-axis, which is invariant under the flow.

We concentrate here on the transition from simple to complex dynamics of the Lorenz equations (1) when the parameter ϱ is varied, while σ and β are kept fixed at the classic values. Figure 1 summarizes the basic information about the bifurcation diagram of the equilibria and periodic orbits as a function of ϱ; see [15, Chapter 6.4] and [33, Chapter 3]. The origin **0** is always an equilibrium with eigenvalues

$$-\beta \quad \text{and} \quad -\frac{1}{2}(\sigma+1) \pm \frac{1}{2}\sqrt{(\sigma+1)^2 + 4\sigma(\varrho-1)}.$$

Hence, **0** is stable for $\varrho < 1$ and becomes a saddle in a pitchfork bifurcation at $\varrho = 1$. For $\varrho > 1$ the origin has a one-dimensional unstable manifold $W^u(\mathbf{0})$ and a two-dimensional stable manifold $W^s(\mathbf{0})$, which we refer to as the *Lorenz manifold*. For $\varrho > 1$ there are two other, secondary equilibria

$$p^{\pm} = (\pm\sqrt{\beta(\varrho-1)}, \pm\sqrt{\beta(\varrho-1)}, \varrho-1)$$

that are each other's image under the symmetry. The secondary equilibria are attractors with a pair of complex conjugate eigenvalues until they lose stability in a subcritical Hopf bifurcation at

$$\varrho_H = \sigma\,(\beta+\sigma+3)\,(\sigma-\beta-1)^{-1} = \frac{470}{19} \approx 24.7368.$$

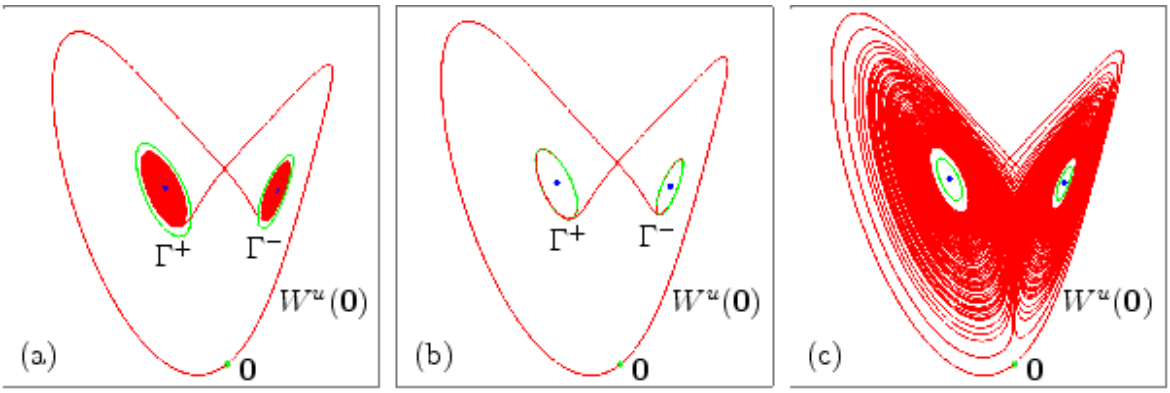

Figure 2. Organisation of the unstable manifold $W^u(\mathbf{0})$ (red curve) for $\varrho = 23.5$ (a), for $\varrho = 24.0579$ (b), and for $\varrho = 24.5$ (c), that is, before, approximately at and and after the heteroclinic bifurcation at $\varrho_{\rm het}$ between the origin $\mathbf{0}$ and the periodic orbits $\Gamma^{\pm}$ (green curves).

Past the Hopf bifurcation for $\varrho > \varrho_H$ the equilibria $p^{\pm}$ are saddle points and have two-dimensional unstable manifolds $W^u(p^{\pm})$, associated with the complex conjugate eigenvalues, and one-dimensional stable manifolds $W^s(p^{\pm})$.

The two saddle periodic orbits $\Gamma^{\pm}$ that bifurcate in the Hopf bifurcation exist in the interval $\varrho_{\mathtt{r}} < \varrho < \varrho_H$. They bifurcate at $\varrho_{\mathtt{r}} \approx 13.9265$ in a symmetrically related pair of homoclinic orbits of the origin; see figure 1. This codimension-one homoclinic bifurcation is also known as a homoclinic explosion point. It is the source of all complicated dynamics in the Lorenz system: for $\varrho > \varrho_{\mathtt{r}} \approx 13.9265$ one finds in a tubular neighbourhood of the two homoclinic loops not only the two periodic orbits $\Gamma^{\pm}$ but also infinitely many other saddle periodic orbits (of well-known symbolic description) [14, 33]. The manifestation of the homoclinic explosion at $\varrho_{\mathtt{r}}$ in terms of the invariant manifolds involved is discussed in detail in section 2.

Note that the homoclinic explosion point at $\varrho_{\mathtt{r}}$ does not produce a chaotic attractor. Rather one initially finds 'preturbulence'in the form of a chaotic transient before the system settles down to one of the attracting equilibria $p^{\pm}$ [18, 33]. At $\varrho_{\rm het} \approx 24.0579$ there is a codimension-one heteroclinic bifurcation that creates a chaotic attractor. At $\varrho_{\rm het}$ there are two symmetrically related heteroclinic orbits between the origin $\mathbf{0}$ and the saddle periodic orbits $\Gamma^{\pm}$. This bifurcation is further illustrated in figure 2. For $\varrho < \varrho_{\rm het}$ the unstable manifold $W^u(\mathbf{0})$ lies in the basin of attraction of the attractors $p^{\pm}$. At the heteroclinic bifurcation at $\varrho_{\rm het}$ the one-dimensional manifold $W^u(\mathbf{0})$ connects $\mathbf{0}$ to the saddle periodic orbits $\Gamma^{\pm}$, that is, $W^u(\mathbf{0})$ is entirely contained in $W^s(\Gamma^{\pm})$. As a result, for $\varrho > \varrho_{\rm het}$ $W^u(\mathbf{0})$ no longer lies in the basin of attraction of $p^{\pm}$, but instead its closure is a chaotic attractor. This chaotic attractor coexists with the attracting equilibria $p^{\pm}$ until they disappear in the Hopf bifurcation at ϱ_H. Hence, for $\varrho > \varrho_H$ the chaotic attractor is the only attractor.

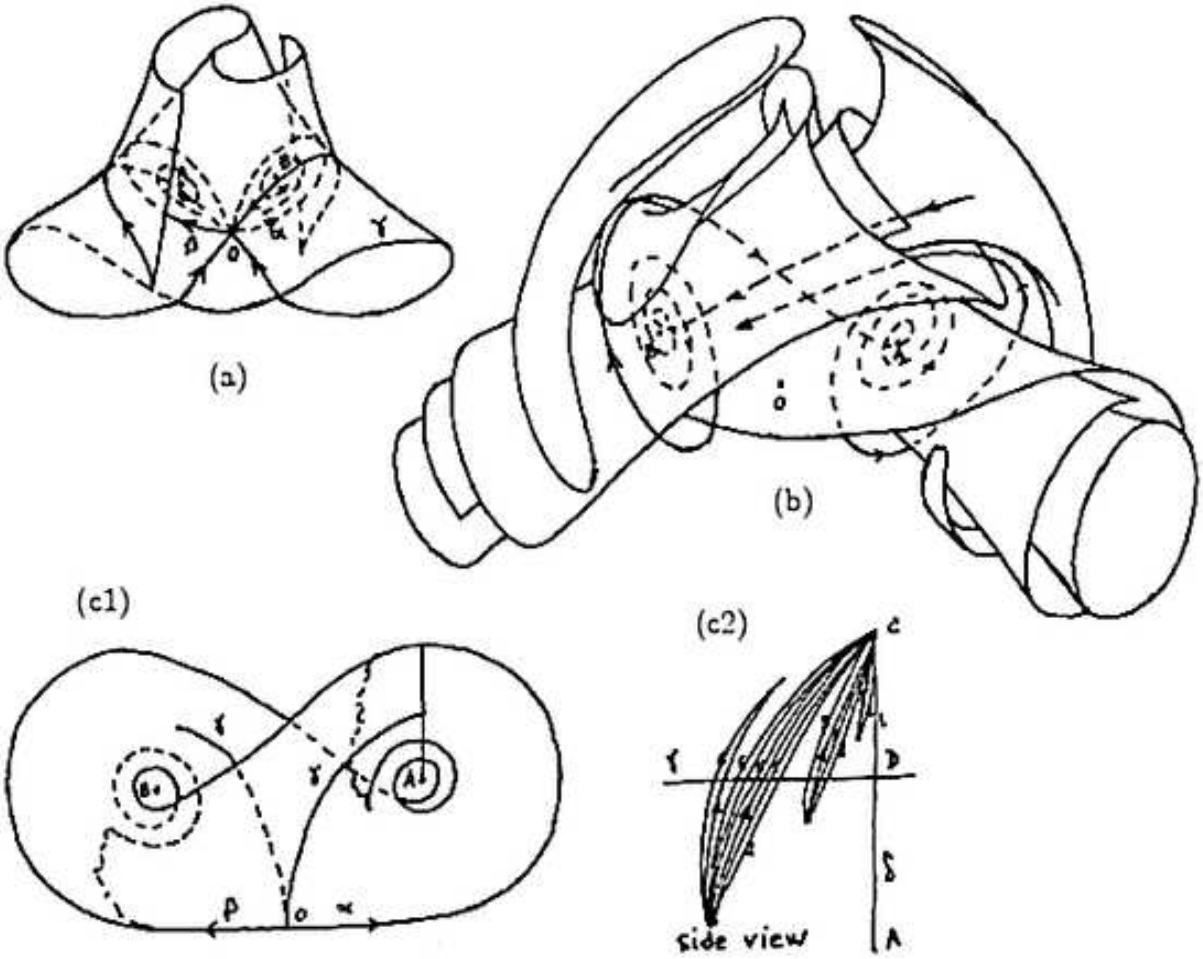

Figure 3. Original sketches by C. Perelló. The Lorenz manifold $W^s(\mathbf{0})$ at the homoclinic explosion (a), and $W^s(\mathbf{0})$ just before the attractors become saddles (b). Panel (c1) shows the unstable manifold $W^s(A)$ of a secondary saddle point A (p^+ in our notation), while panel (c2) illustrates its multi-sheeted nature.
Reproduced with kind permission of Springer Science and Business Media from C. Perelló, Intertwining invariant manifolds and the Lorenz attractor, in *Global theory of dynamical systems (Proc. Internat. Conf., Northwestern Univ., Evanston, Ill., 1979)*, Lecture Notes in Math. **819**, Springer-Verlag, Berlin, pp. 375–378. ©1979 Springer-Verlag.

In this paper we address the question of how the transition through the homoclinic explosion and beyond manifests itself in terms of the organisation of the respective two-dimensional invariant manifolds of $\mathbf{0}$, $p^{\pm}$ and $\Gamma^{\pm}$. Specifically, in section 2 we compute $W^s(\mathbf{0})$, $W^u(p^{\pm})$ and $W^u(\Gamma^{\pm})$ for different values of ϱ with specialized software that has become available only in recent years; see the survey [22]. We use the geodesic level set (GLS) method of [19, 20] for computing $W^s(\mathbf{0})$ and a boundary value problem (BVP) approach (see [22, Sec. 3]) for computing $W^u(p^{\pm})$ and $W^u(\Gamma^{\pm})$, respectively. This allows us to study how the global manifolds and their intersections change with the parameter ϱ. In section 3 we use a boundary value approach to find the first 512 of the infinitely many codimension-zero heteroclinic orbits that form the intersection

between $W^s(\mathbf{0})$ and $W^u(p^\pm)$ for $\varrho = 28.0$. We introduce their symbolic structure and then, in section 4, continue all 512 heteroclinic orbits in ϱ. All these heteroclinic orbits are born in the homoclinic explosion point $\varrho_{\mathtt{r}} \approx 13.9265$. When continued for increasing ϱ each branch of heteroclinic orbits has a fold and ends at a specific value of ϱ in another codimension-one homoclinic bifurcation. As is discussed in section 5, each of these homoclinic bifurcations is also a homoclinic explosion point with a well-defined symbol sequence. We give a complete description in terms of symbol sequences of which heteroclinic orbits end at which homoclinic explosion points.

There is an enormous amount of literature on the Lorenz equations. We finish this introduction by reviewing briefly some key references of direct relevance to the results in this paper. A more detailed discussion of how the symbolic dynamics of heteroclinic orbits discussed here relates to previous work on the symbolic dynamics of periodic obits can be found in section 6.

As far as we are aware, Perelló [30] is the only one who considered directly the dependence of the Lorenz manifold $W^s(\mathbf{0})$ on the parameter ϱ, including the transition through the homoclinic explosion. In fact, he produced the first ever three-dimensional drawings of $W^s(\mathbf{0})$, which are reproduced in figure 3. The drawing in figure 3(a) shows the geometry of $W^s(\mathbf{0})$ at the homoclinic explosion point at $\varrho_{\mathtt{r}}$, while figure 3(b) shows $W^s(\mathbf{0})$ just before the attractors become saddles. In fact, this drawing was a basis for the illustrations by Abraham and Shaw [1] of the Lorenz manifold for $\varrho = 28.0$. Notice the emphasis on the two scrolls of $W^s(\mathbf{0})$ around the one-dimensional stable manifolds of the secondary equilibria. The question of what this means for the overall geometry of $W^s(\mathbf{0})$ was answered only quite recently when a sufficiently large piece of $W^s(\mathbf{0})$ could be computed [21, 22, 27]. Perelló also considered the unstable manifold of the secondary equilibria. Figure 3(c) shows a part of $W^u(p^+)$ and how it is bounded by $W^u(\mathbf{0})$. It was obtained by Perelló by "saturating" a line segment, which is remarkably close to our approach of computing $W^u(p^+)$; see section 2.2.

There is quite some literature on the symbolic description of the Lorenz system, namely to characterize the periodic orbits on the Lorenz attractor and their bifurcations. Guckenheimer and Williams [16, 37], Afrajmovich, Bykov and Sil'nikov [2], and Rand [31] introduced and studied a one-dimensional discontinuous map model of the attractor, called the *geometric Lorenz attractor*. The geometric Lorenz attractor describes the dynamics on the intersection of the Lorenz attractor with the Poincaré section $\Sigma_\varrho = \{z = \varrho - 1\}$ through the secondary equilibria. The discontinuous one-dimensional map (describing how leaves of the strong stable foliation map to one another) has a left and a right branch, which defines the itinerary or kneading sequence of any point under the dynamics in terms of an infinite sequence of `l`s and `r`s (denoting application of the respective branch). The chaotic dynamics arises in the geometric Lorenz attractor just as we just described for the Lorenz system, namely via the equivalents of the basic homoclinic explosion, heteroclinic bifurcation, and Hopf bifurcation; see [15, Chapter 6.4] and [33, Chapter 3.4].

Closely related to the geometric Lorenz attractor is the concept of the *template* of the Lorenz system, which is a branched two-manifold that allows one to describe the symbolic dynamics of the knot-types in $\mathbb{R}^3$ of periodic orbits on the Lorenz attractor; see the original paper by Lorenz [24], the work by Ghrist *et al.* [12, 38], and the recent textbook [13]. In fact, figure 3(c1) by Perelló nicely illustrates the Lorenz template, which is effectively obtained by identifying the infinitely many (local) sheets that meet along the initial piece of the unstable manifold $W^u(\mathbf{0})$; see also figure 7 below. The chaotic nature of the Lorenz system (for the classic parameter values) was proved by Tucker [34] only quite recently by showing with computer-assisted rigorous estimates that the Lorenz attractor indeed satisfies the technical conditions needed in the reduction to the geometric Lorenz attractor; see also the review by Viana [35]. Therefore, properties of the geometric Lorenz attractor carry over to the Lorenz system, which can be exploited to show properties of the attractor; see, for example, the recent result on mixing by Luzatto *et al.* [25].

While the results mentioned above are quite theoretical in nature, there have been a number of investigations of periodic orbits of the Lorenz system that also involve numerical tools. The periodic orbits of the Lorenz attractor itself (for fixed $\varrho = 28.0$) have been computed systematically with varying accuracy and up to different lengths of their (repeating) symbol sequences. Franceschini *et al.* [11] computed all periodic orbits with up to 9 symbols and Eckhardt and Ott [8] all periodic orbits with up to 11 symbols. Viswanath [36] builds up longer periodic orbits recursively from shorter ones and computes all periodic orbits with up to 20 symbols, as well as some with very long symbol sequences (up to 347 symbols).

A more general topic is the dependence of the periodic orbits on parameters. A wealth of information on this subject is contained in Sparrow's book [33]. By means of careful investigations with numerical integration in combination with theoretical results from bifurcation theory, he gives a consistent picture in terms of symbol sequences of the periodic orbits in the dependence on the parameter ϱ. The periodic orbits can be followed from the basic homoclinic explosion point at $\varrho_{\mathtt{r}}$ towards larger values of ϱ and through folds back to different homoclinic explosion points. New branches are born in period-doubling bifurcations and also end at homoclinic explosion points. These results in [33] are summarized in a bifurcation diagram of periodic orbits with different symbol sequences; see also [13]. Note that [33] also contains information on the dependence of the system on other parameters, including results on the limits of large ϱ and small β, as well as conjectured bifurcaton diagrams in the (β, ϱ)-plane (for the classic value of $\sigma = 10$); see also the work by Robbins [32]. Recently, Dullin *et al.* [7] considered the entire (ϱ, σ)-plane and found an alternating periodic pattern of stability regions of symmetric and non-symmetric periodic orbits, which they explain by considering certain limits of large ϱ and σ.

Overall, the work presented here is quite similar in spirit to that by Perelló and Sparrow. The sketches in figure 3 were developed by Perelló with the help of representative trajectories generated on a "desktop computer with a plotter" [30].

Similarly, the bifurcation diagrams of periodic orbits versus ϱ and the determination of their symbolic dynamics by Sparrow [33] were obtained with a systematic numerical exploration by means of numerical integration guided by theoretical insight and expectation. Both Perelló and Sparrow used state-of-the-art numerical tools at the time, namely numerical integration to solve initial value problems. Similarly, we use state-of-the-art numerical tools of today, most importantly manifold computation and the continuation of solutions of suitable boundary value problems. Only with the development of these tools has it become possible to investigate in detail how the Lorenz manifold $W^s(\mathbf{0})$ interacts with $W^u(p^\pm)$ and $W^u(\Gamma^\pm)$. Therefore, in many respects our work continues from and complements their earlier work.

2. Dependence of the manifolds on ϱ

For the standard value of $\varrho = 28.0$ the Lorenz system has a strange attractor which is the global attractor of the system. The global dynamics of how trajectories spiral into the Lorenz attractor is organized by the Lorenz manifold $W^s(\mathbf{0})$, which essentially separates trajectories that follow the left branch or the right branch of $W^u(\mathbf{0})$, respectively, when they pass close to the origin $\mathbf{0}$. From a geometrical point of view, computed up to fixed geodesic distance, the two-dimensional surface $W^s(\mathbf{0})$ is the smooth image of a disk that simultaneously 'rolls' into the right and left 'wing' of the Lorenz attractor. As is now known, this results in a primary helix along the positive z-axis, with infinitely many secondary helices close to this primary helix; for more information on the geometry of the Lorenz manifold see [21, 27, 28].

In this section we consider how the Lorenz manifold $W^s(\mathbf{0})$ changes when ϱ is decreased through the bifurcation diagram in figure 1. Similarily we study how the unstable manifolds $W^u(p^\pm)$ and $W^u(\Gamma^\pm)$, respectively, change in this transition.

2.1. The stable manifold $W^s(\mathbf{0})$

Figure 4 shows four images of $W^s(\mathbf{0})$ for different values of ϱ as computed with the GLS method of [20] in the implementation described in [10] (which uses `AUTO`'s collocation and pathfollowing routines). All four manifolds were computed up to geodesic distance 100.0, so include the z-axis from $(0, 0, -100.0)$ to $(0, 0, +100.0)$. We coloured $W^s(\mathbf{0})$ in shades that get paler as the geodesic distance increases; the boundary of $W^s(\mathbf{0})$, that is, the geodesic level set of distance 100, is drawn as a darker curve. The changes of the manifold with ϱ is best seen in the accompanying `animation 1`. In particular, the torsion of the helix around the positive z-axis increases as ϱ decreases.

Figure 4(a) shows the Lorenz manifold $W^s(\mathbf{0})$ for the classical value of $\varrho = 28.0$. The manifold rolls up around the one-dimensional stable manifolds $W^s(p^\pm)$ (not shown) of the secondary equilibria $p_\pm$ and thereby forms the primary helix along the positive z-axis. Until the Hopf bifurcation at $\varrho_H \approx 24.7368$, the situation remains topologically the same. Then the saddles $p^\pm$ become attractors that co-exist with the Lorenz attractor.

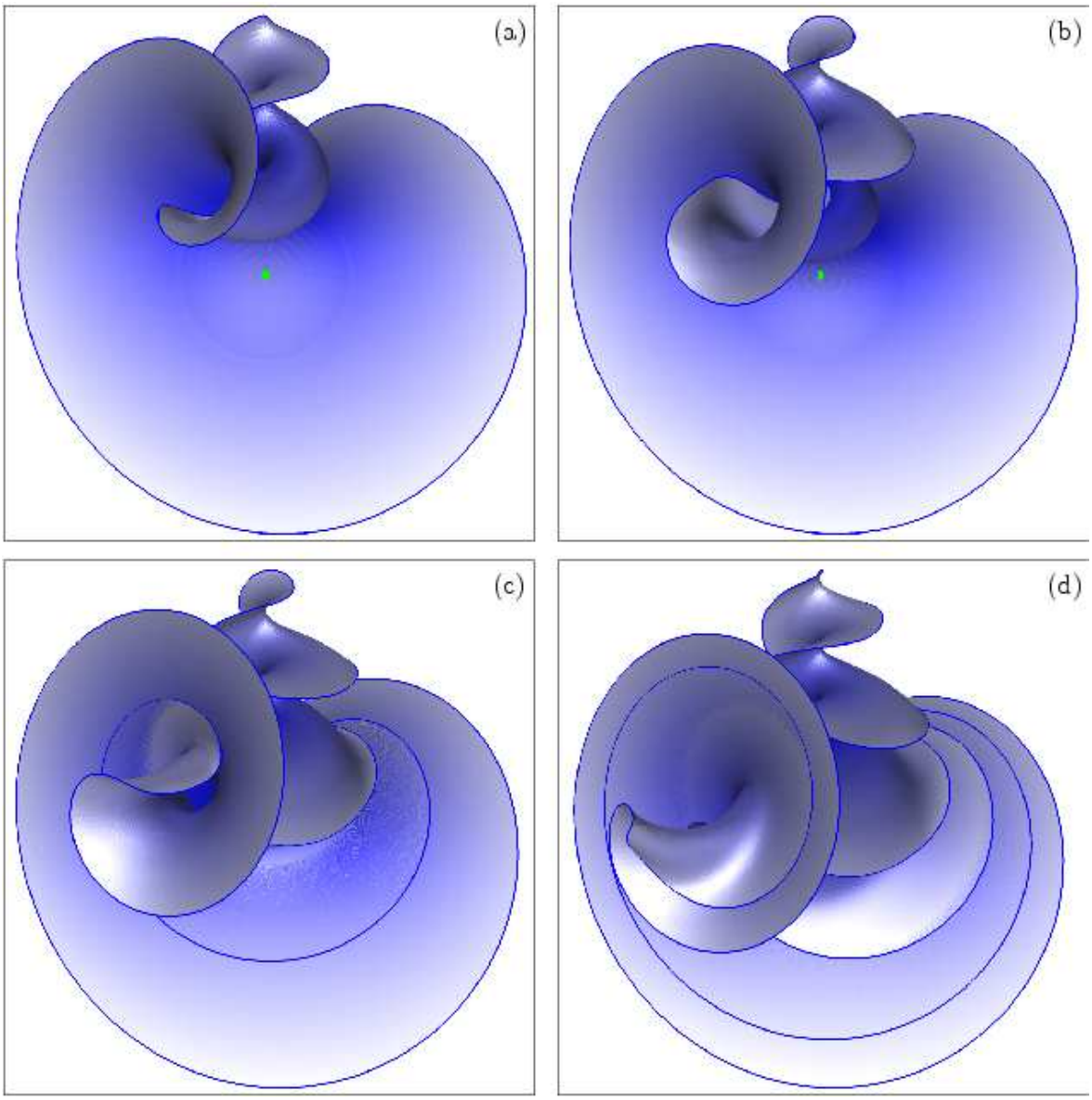

Figure 4. The manifold $W^s(\mathbf{0})$ up to geodesic distance 100 for $\varrho = 28.0$ (a), for $\varrho = 19.0$ (b), for $\varrho = 10.0$ (c), and for $\varrho = 1.0$ (d). To help identify the changes to $W^s(\mathbf{0})$ the shade of blue changes from darker to lighter as the geodesic distance increases and the boundary at geodesic distance 100 is highlighted as a dark blue curve; see also the accompanying `animation 1`.

The Lorenz manifold $W^s(\mathbf{0})$ now rolls around the stable manifolds $W^s(\Gamma^{\pm})$ (not shown) of the saddle periodic orbits $\Gamma^{\pm}$, which form the basin boundaries of $p^{\pm}$. As an example, the manifold for $\varrho = 19.0$ is shown in figure 4(b) and, in fact, this is the situation sketched by Perelló in figure 3(b). We remark that the transition through the Hopf bifurcation results in a continuous deformation of $W^s(\mathbf{0})$.

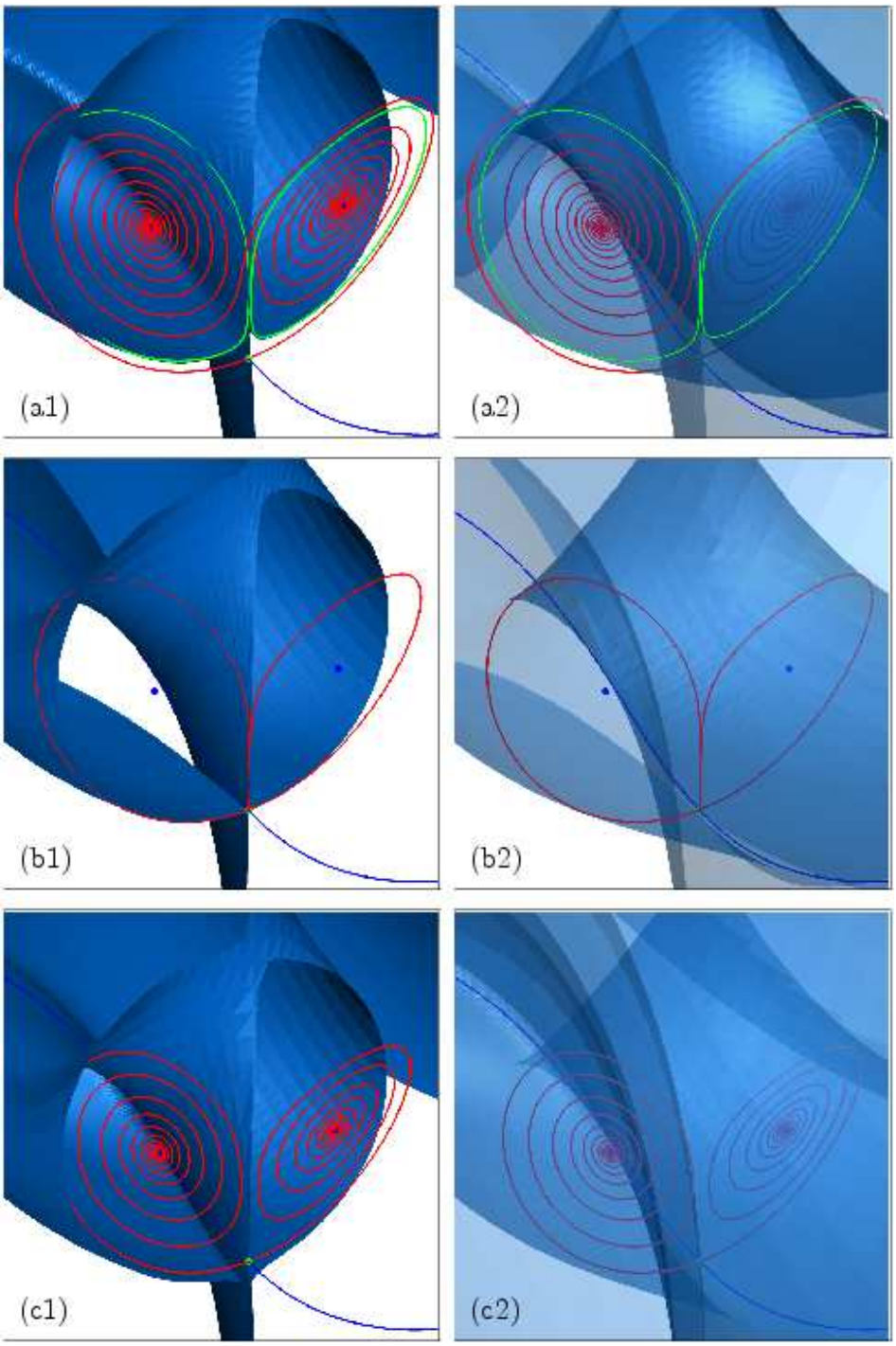

Figure 5. Organisation of manifolds $W^s(\mathbf{0})$ (blue surface), $W^{ss}(\mathbf{0})$ (blue curve) and $W^u(\mathbf{0})$ (red curve) for $\varrho = 15.0$ (a), for $\varrho = 13.9265$ (b), and for $\varrho = 13.0$ (c), that is, before, approximately at, and after the homoclinic bifurcation. On the left $W^s(\mathbf{0})$ is clipped along a plane spanned by the z-axis and the unstable eigenvector of the origin, and on the right it is rendered transparent. In row (b) $W^s(\mathbf{0})$ is of geodesic distance 64.175 and in rows (a) and (c) it is of geodesic distance 100.0. Row (a) also shows the two bifurcating saddle periodic orbits $\Gamma_\pm$ (green curves).

The transformation through the homoclinic explosion at $\varrho_{\mathtt{r}} \approx 13.9265$, on the other hand, results in a more dramatic change of $W^s(\mathbf{0})$. When ϱ is decreased from 24.7368 towards this homoclinic bifurcation point, the saddle periodic orbits $\Gamma^{\pm}$ grow larger in radius, while $W^s(\mathbf{0})$ rolls around $\Gamma^{\pm}$ and $W^s(\Gamma^{\pm})$. At $\varrho_{\mathtt{r}}$ the unstable manifold $W^u(\mathbf{0})$ lies in $W^s(\mathbf{0})$ and forms a homoclinic loop. At this moment $W^s(\mathbf{0})$ is degenerate. It rolls around $p^{\pm}$ exactly once and ends along the strong stable manifold $W^{\mathrm{ss}}(\mathbf{0}) \in W^s(\mathbf{0})$. For $\varrho < 13.9265$ the Lorenz manifold $W^s(\mathbf{0})$ rolls around $p^{\pm}$ exactly once, after which it turns back along itself exponentially closely toward the direction of negative z. This change of the manifold can be seen clearly in figure 4(c) and (d). Notice the parts of the boundary of $W^s(\mathbf{0})$ that now lie in the region of negative z, indicating that there are now several sheets of the computed manifold in this region.

Figure 5 shows the transition through the homoclinic explosion at $\varrho_{\mathtt{r}}$ in more detail. Shown are the stable and unstable manifolds $W^s(\mathbf{0})$ and $W^u(\mathbf{0})$ for $\varrho = 15.0$, 13.9265, and 13.0; the one-dimensional blue curve is the strong stable manifold $W^{\mathrm{ss}}(\mathbf{0})$. Note that we describe the transition through the homoclinic bifurcation for decreasing ϱ to be consistent with figure 4. In the left column of figure 5 only the part of $W^s(\mathbf{0})$ is shown that lies 'behind' the plane normal to $\vec{n} := v^u(\mathbf{0}) \times (0,0,1)^T$ through the point $0.1\,\vec{n}$. That is, we clip $W^s(\mathbf{0})$ with the plane spanned by the z-axis and the unstable eigenvector $v^u(\mathbf{0})$. The right column of figure 5 shows $W^s(\mathbf{0})$ in transparent blue. The manifold $W^s(\mathbf{0})$ was computed up to geodesic distance 100.0 for $\varrho = 13.0$ and 15.0; for $\varrho = 13.9265$ it was computed up to geodesic distance 64.175.

Figure 5(a) shows the situation for $\varrho = 15.0$ with the pair of periodic orbits $\Gamma^{\pm}$ already approaching the origin quite closely. Observe how $W^s(\mathbf{0})$ returns close to the origin and then turns upwards (towards positive values of z): effectively, $W^s(\mathbf{0})$ rolls around $\Gamma^{\pm}$ infinitely many times. Notice that the unstable manifold $W^u(\mathbf{0})$ 'crosses behind' $W^u(\mathbf{0})$, so that its left branch accumulates on the attractor p^+ and its right branch on p^-. Figure 5(b) shows the situation (approximately) at the homoclinic explosion for $\varrho = 13.9265$. The two branches of $W^u(\mathbf{0})$ no longer accumulate on $p^{\pm}$, but come back to the origin to form two (symmetrically related) homoclinic orbits, being entirely contained in $W^s(\mathbf{0})$; see panel (b2). The Lorenz manifold $W^s(\mathbf{0})$ was computed up to the geodesic distance 64.175 when it comes back to the origin along the homoclinic orbit. Indeed $W^s(\mathbf{0})$ cannot be parametrized by smooth geodesic level sets for larger geodesic distances. Rather, this two-dimensional manifold aligns with and 'closes up', much like a zipper, along $W^{ss}(\mathbf{0})$. Figure 5(c) shows the situation for $\varrho = 13.0$. The equilibria $p^{\pm}$ are now the only attractors and $W^s(\mathbf{0})$ separates their respective basins of attraction. Now the left branch of $W^u(\mathbf{0})$ spirals directly into p^- and the right branch directly into p^+. The Lorenz manifold $W^s(\mathbf{0})$ folds around $p^{\pm}$ once, comes very close to the origin, or more precisely close to $W^{\mathrm{ss}}(\mathbf{0})$, and then, rather than making another revolution around $p^{\pm}$, folds away downwards (towards negative values of z) and back along itself; see panel (c1) and compare with Figure 4(c) and (d). In particular, all trajectories on $W^s(\mathbf{0})$ go to infinity in backward time.

2.2. The unstable manifolds $W^u(p^\pm)$ and $W^u(\Gamma^\pm)$

For $\rho = 28.0$ the unstable manifolds $W^u(p^\pm)$, which are each other's image under the symmetry, both accumulate on the Lorenz butterfly attractor. The local manifolds near $p^\pm$ are approximate nice disks but, as they grow and accumulate on the Lorenz attractor, they each pass back and forth infinitely many times between the two wings of the attractor. In other word, $W^u(p^\pm)$ has infinitely many sheets, which are actually extremely close together due to the contraction rates involved. Collapsing these sheets leads to the well-known template of the Lorenz system in the form of a branched surface [12, 13].

When ϱ is decreased below the Hopf bifurcation at $\varrho_H \approx 24.7368$ then $W^u(p^\pm)$ transforms into $W^u(\Gamma^\pm)$. Locally near $\Gamma^\pm$ this manifold now has two parts, one inside and one outside $W^s(\Gamma^\pm)$. The inside branch is a topological disk that has the attractor $p^\pm$ as its closure, while the outside branch is as complicated as $W^u(p^\pm)$ for $\varrho > 24.7368$. When ϱ is decreased further, the periodic orbits $\Gamma^\pm$ grow until they finally disappear in the explosion point at $\varrho_{\mathtt{r}} \approx 13.9265$. The manifolds $W^s(\Gamma^\pm)$ also cease to exist in this bifurcation.

Computing a good representation of $W^u(p^\pm)$ and $W^u(\Gamma^\pm)$ is quite a challenge. Due to extreme folding of the manifolds the GLS or other growth methods quickly run into difficulties. As an alternative we find and continue suitable orbit segments with a BVP approach [22, Sec. 3]. Specifically, we compute two families of orbit segments as shown in figure 6 for $\varrho = 28.0$ with the package `AUTO` [4]. Both families start along a vector in the linear unstable eigenspace of p^+; in fact the end points of the orbit segments hardly change and are marked by a diamond. The orbit segments in figure 6(a) spiral around p^+ a number of times, then make one revolution around p^- and end in the section $\Sigma_\varrho = \{z = \varrho - 1\}$ (on the far side of p^+). Similarly, the orbit segments in figure 6(b) spiral around p^+ a number of times, then make one and a half revolutions around p^- and end in Σ_ϱ (on the far side of p^-). Starting from an orbit segment found by continuation in the integration time T, the respective families are then continued as two-point boundary value problems with `AUTO`.

The two families (represented by black curves) are bounded by the purple and red orbits in figure 6, which are concatenations of a heteroclinic orbit from p^+ to the origin $\mathbf{0}$ with a piece of $W^u(\mathbf{0})$. The heteroclinic part of the two purple orbits makes infinitely many revolutions around p^+ before ending up at $\mathbf{0}$ (symbolized by `R`), while the heteroclinic part of the two red orbits also makes a single revolution around p^- before ending up at $\mathbf{0}$ (symbolized by `Rl`). These heteroclinic orbits are intersection curves (of codimension zero) of $W^u(p^+)$ with $W^s(\mathbf{0})$. As we discuss in detail in section 4, infinitely many such heteroclinic orbits with a well-defined symbolic description organize the intersections between $W^s(\mathbf{0})$ and $W^u(p^\pm)$ and $W^u(\Gamma^\pm)$, respectively.

The families of orbit segments in figure 6 were used to render the manifolds $W^u(p^+)$ and $W^u(p^-)$ (by symmetry) as surfaces. Taken together, they constitute a numerical version of the template of the Lorenz system. In fact, we chose the families of orbit

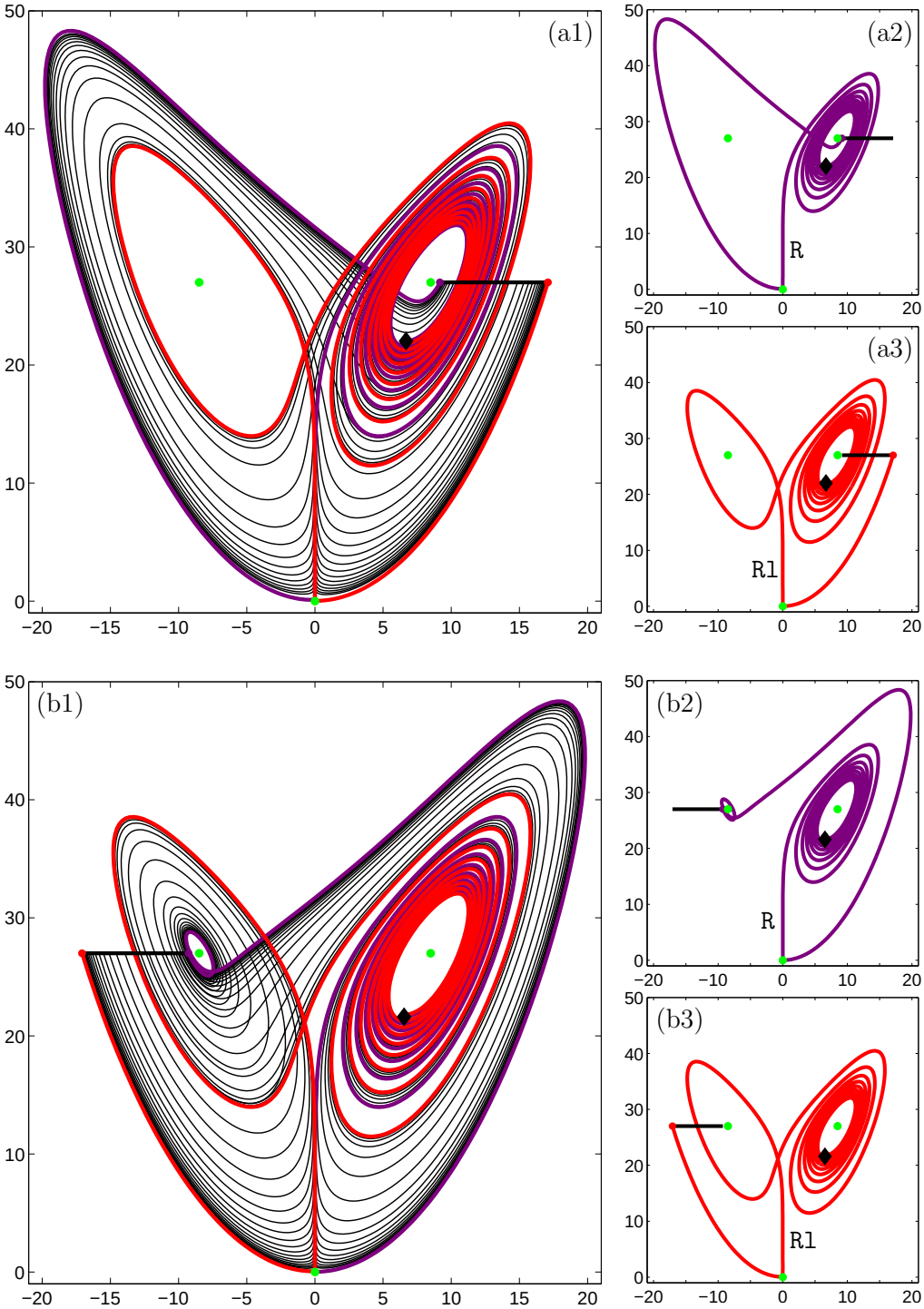

Figure 6. Two families of orbit segments were used to compute (a part of) $W^u(p^+)$ or $W^u(\Gamma^+)$; the example shown is for $\varrho = 28.0$. The orbits segments start in the unstable eigenspace (near $\diamond$) of $W^u(p^+)$ and end in the section $\{z = \varrho - 1\}$, either near p^+ (a1) or near p^- (b1). Both families limit on the two singular orbit segments in panels (a2)/(a3) and (b2)/(b3), which are composed of a heteroclinic orbit (of type `R` and `Rl`, respectively) composed with an initial piece of $W^u(\mathbf{0})$.

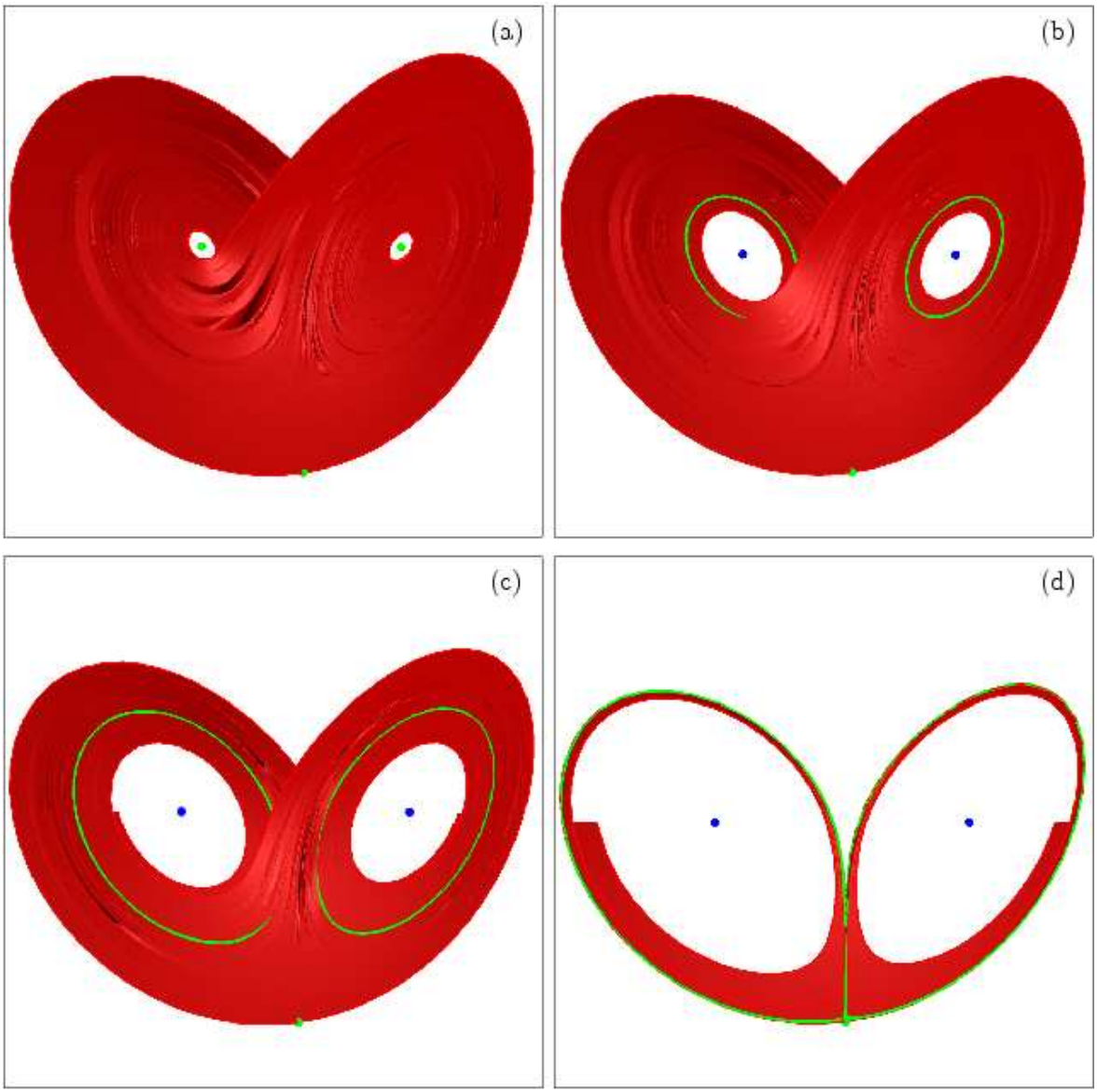

Figure 7. The manifolds $W^u(p^{\pm})$ for $\varrho = 28.0$ (a), and $W^u(\Gamma^{\pm})$ for $\varrho = 23.0$ (b), $\varrho = 19.0$ (c), and $\varrho = 14.0$ (d), respectively, as rendered from the families of orbit segments in figure 6; see also the accompanying `animation 2`.

segments such that they encode the 'switching from right to left' that is the hallmark of this template. We remark that we used the same families also to compute $W^u(\Gamma^{\pm})$ (for lower values of ϱ).

Figure 7 and the accompanying `animation 2` show how $W^u(p^{\pm})$ and $W^u(\Gamma^{\pm})$ change with ϱ. Note that the holes around the secondary equilibria $p^{\pm}$ in figure 7 could be filled with simple disks. However, we felt that it is better to show only the computed orbit families, as this also emphasizes the dynamics on $W^u(p^{\pm})$ and $W^u(\Gamma^{\pm})$. In figure 7(a) for the classical value of $\varrho = 28.0$ one can recognise the computed part of $W^u(p^{\pm})$ as forming the template of the Lorenz system. In effect, each family of orbit segments transports (backward in time) the respective one-dimensional intersection

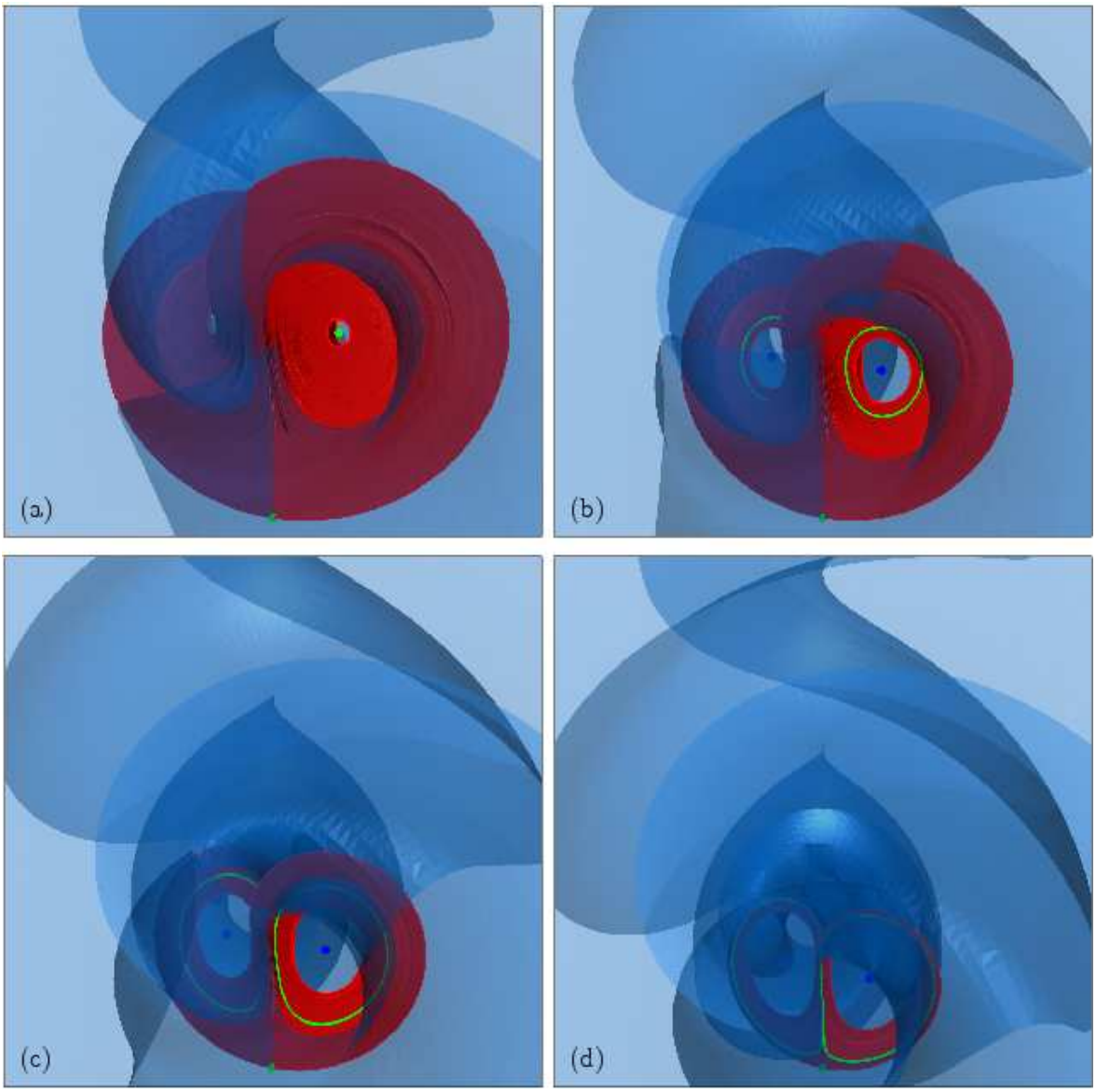

Figure 8. A transparent rendering of $W^s(\mathbf{0})$ (blue surface) as it intersects the unstable manifolds (red surfaces) $W^u(p^\pm)$ for $\varrho = 28.0$ (a), and $W^u(\Gamma^\pm)$ for $\varrho = 23.0$ (b), $\varrho = 19.0$ (c), and $\varrho = 15.0$ (d), respectively; see also the accompanying animation.

curve $W^u(p^\pm) \cup \Sigma_\varrho$. In this sense, our method of computing $W^u(p^\pm)$ is similar to Perelló's method of 'saturating' a line segment; compare figure 7(a) with figure 3(c). In particular, the computed part of $W^u(p^\pm)$ is bounded by $W^u(\mathbf{0})$. Figure 7(b) shows the computed part of $W^u(\Gamma^\pm)$ for $\varrho = 23.0$, which is still bounded by $W^u(\mathbf{0})$. As ϱ is decreased further to $\varrho = 19.0$ in figure 7(c), the holes around $p^\pm$ grow, which indicates that the orbit families we considered cover less and less of $W^u(\Gamma^\pm)$. In fact, as is illustrated in figure 7(c) for $\varrho = 14.0$ very near the homoclinic bifurcation, the computed families of orbit segments have the homoclinic orbits as their limit.

Figure 8 and the accompanying `animation 3` show $W^s(\mathbf{0})$ together with $W^u(p^\pm)$ and $W^u(\Gamma^\pm)$, respectively, as ϱ is changed. Here $W^s(\mathbf{0})$ is rendered transparent and

all panels show the same part of the phase space. Notice how $W^u(\Gamma^\pm)$ become smaller and then disappear for decreasing ϱ. The two sets of manifolds intersect in infinitely many codimension-one heteroclinic orbits; the purple and red orbits in figure 6 are two concrete examples.

3. Generic heteroclinic orbits for $\varrho = 28.0$

While figure 8 gives a good impression of the overall geometric arrangment of the manifolds, it is practically impossible to resolve from this figure the heteroclinic orbits that form the intersection set. Therefore, we now adopt the approach of identifying the generic heteroclinic orbits for $\varrho = 28.0$ directly with a continuation method. In the next section we then follow these heteroclinic orbits in the parameter ϱ.

Specifically, we fix $\varrho = 28.0$ and systematically find the heteroclinic orbits from the secondary equilibrium p^+ to the origin as follows. First we perform a continuation with `AUTO` [4] in integration time (parameter T) where we start from an initial condition along a particular direction in the unstable eigenspace $E^u(p^+)$ at distance r_0 from p^+. We then fix the integration time T at a suitable value and continue the initial orbit segment in the parameter r_0. During this continuation the orbit segment sweeps over $W^u(p^+)$ and, hence, also over the heteroclinic orbits we are seeking. Importantly, the heteroclinic orbits stand out as local minima of the arclength, as well as the L_2 or integral norm, because most of the integration time T is spent near the origin. Since the orbit spirals near p^+, the result of the continuation effectively repeats itself after r_0 has covered a fundamental domain. In our procedure a fundamental domain can be defined conveniently as the r_0-range between successive detections of the basic heteroclinic orbit that spirals around $p^\pm$ and then connects directly to the origin, which has the overall smallest norm of any orbit.

Figure 9 shows the norm of the resulting family of orbit segments for fixed T over a fundamental domain in r_0. The (approximate) heteroclinic orbits from p^+ to $\mathbf{0}$ are clearly identified as very distinct local minima. What is more, figure 9 brings out the tree structure of the heteroclinic orbits, which is directly related to their description by symbol sequences.

We introduce a symbolic coding for heteroclinic orbits that is very similar to what has been used for periodic orbits; see [33] and also [36]. We refer to p^- and p^+ as the left (`l`) and right (`r`) equilibria and use `R` as an abbreviation for infinitely many revolutions around p^+. The basic heteroclinic orbit connects p^+ directly with $\mathbf{0}$ and has the symbol sequence `R`.

For any other heteroclinic orbit infinitely many revolutions around p^+ are followed by an initial (0th) revolution around p^-. Then follow finitely many revolutions in some order around p^+ or p^- before the heteroclinic orbit ends at $\mathbf{0}$. Therefore, its symbol sequence is defined as

$$\texttt{Rl}s_1 \cdots s_N, \quad \text{where} \begin{cases} s_j = \texttt{l} & \text{if the } j\text{th revolution is around } p^-, \\ s_j = \texttt{r} & \text{if the } j\text{th revolution is around } p^+. \end{cases} \tag{2}$$

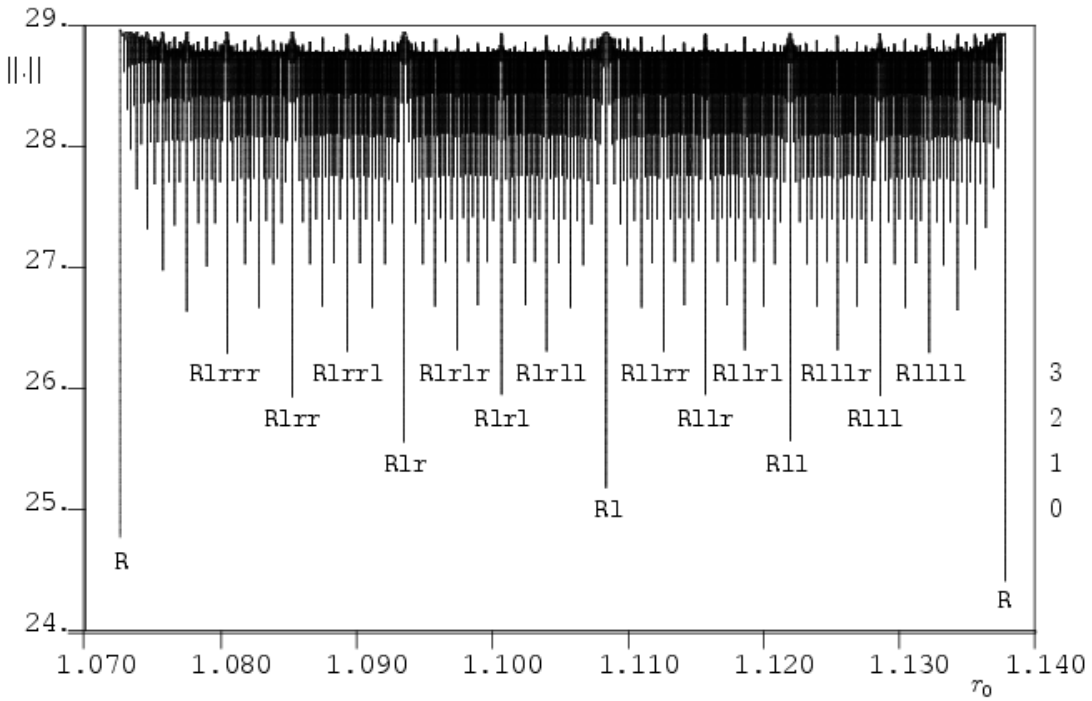

Figure 9. Family for $\varrho = 28.0$ of orbit segments of fixed time $T = 30.1473$ that start at distance r_0 along a vector in $E^u(p^+)$. Local minima of the integral norm $||.||$ correspond to (approximate) heteroclinic orbits from p^+ to $\mathbf{0}$; their symbol sequences for levels 0 to 3 are shown. The continuation in r_0 covers one fundamental domain, starting and ending at the basic heteroclinic orbit `R`.

Here, N is the number of subsequent revolutions around p^- and p^+, to which we refer as the *level* of the symbol sequence or heteroclinic orbit. Symbol sequences for heteroclinic orbits from p^- to the origin are defined in complete analogy, where we use `L` as an abbreviation of the initial infinitely many revolutions around p^-. Due to the symmetry of the Lorenz equations, for every heteroclinic orbit with sequence $\mathtt{Rl}s_1 \cdots s_N$ there exists the symmetrically related heteroclinic orbit with sequence $\mathtt{Lr}\overline{s}_1 \cdots \overline{s}_N$, where $\overline{\mathtt{r}} = \mathtt{l}$ and $\overline{\mathtt{l}} = \mathtt{r}$.

The notion of a revolution around the points p^+ or p^- can be made precise: each such revolution corresponds to a unique intersection point of the heteroclinic orbit with the section Σ_ρ (located at the height of the secondary equilibria) where the flow is pointing upwards (in the direction of increasing z). Note that this definition agrees with the symbol sequences as used for the approximation of the return map of (1) on the section Σ_ϱ by a one-dimensional discontinuous map (see [16] and [33, Chapter 3.4]), where `l` corresponds to the left branch and `r` to the right branch of the map.

One key aspect of definition (2) is that the symbol sequence of a heteroclinic orbit can be extracted automatically from the approximating orbit segment. Figure 10 shows as examples the heteroclinic orbits `Rl` (row a) and `Rrlrlllr` (row b) in phase space and as a time series of the x-value. Notice how the symbolic code can be determined easily

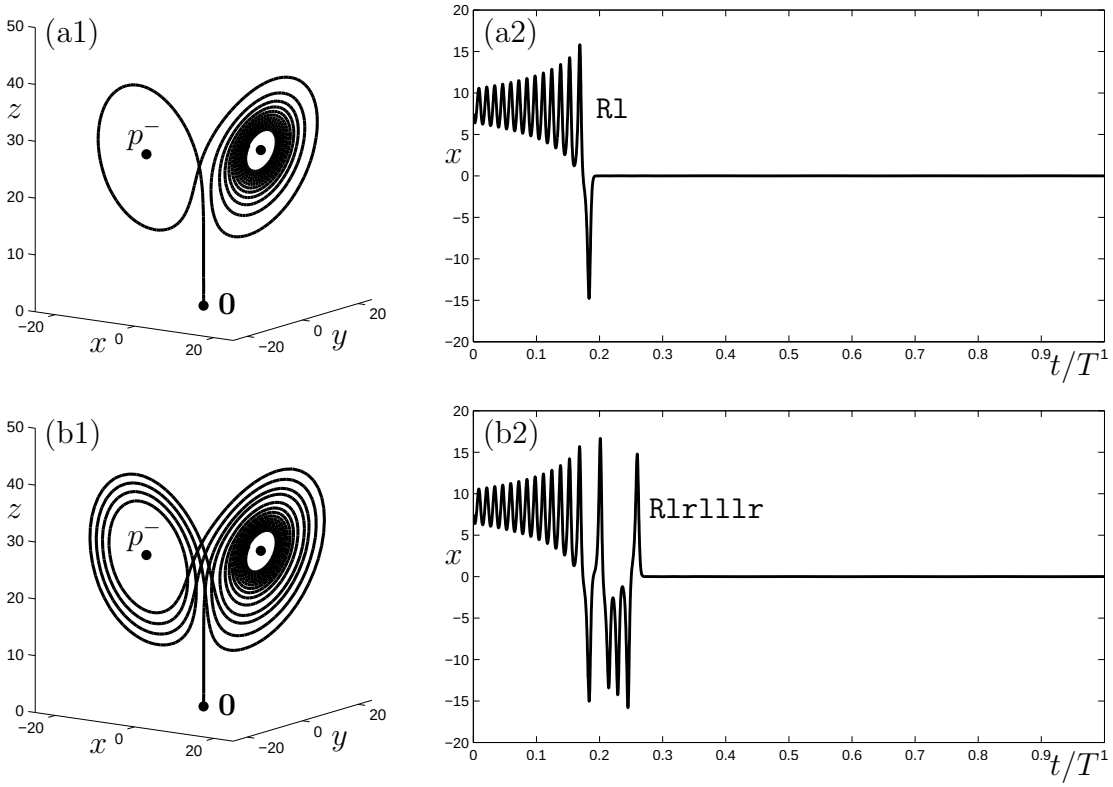

Figure 10. The heteroclinic orbits from p^+ to **0** of (1) for $\varrho = 28.0$ with symbolic sequences `Rl` (a) and `Rlrlllr` (b), shown in phase space (left) and as time series of the x-value (right).

from the plot of the x-coordinate versus rescaled time t/T.

In figure 9 the basic heteroclinic orbit `R` and all non-basic heteroclinic orbits of levels 0 to 3 are labelled. The family of orbit segments shown in figure 9 actually allowed us to extract automatically all heteroclinic orbits and symbolic sequences up to level 8. We found 2^i in all levels for $i \leq 8$, a total of 512 heteroclinic orbits. Figure 9 also constitutes clear numerical evidence that, as a function of the parameter r_0, the heteroclinic orbits on $W^u(p^+)$ actually occur in the *recursive ordering on a full binary tree*, which can be defined formally as follows.

Definition Given two symbol sequences $\mathtt{R}s_0 \cdots s_N$ and $\mathtt{R}t_0 \cdots t_M$ where $s_j, t_j \in \{\mathtt{r}, \mathtt{l}\}$ let $0 \leq k \leq \min(N, M)$ be the largest integer such that $s_j = t_j$ for $0 \leq j \leq k$. Then

$$\mathtt{R}s_0 \cdots s_N < \mathtt{R}t_0 \cdots t_M \quad \text{if} \quad \begin{cases} s_{k+1} = \mathtt{l}, t_{k+1} = \mathtt{r} \text{ and } k < \min(N, M), \\ s_{k+1} = \mathtt{l} \text{ and } k = M, \\ t_{k+1} = \mathtt{r} \text{ and } k = N. \end{cases} \tag{3}$$

The ordering can be described locally as

$$\mathtt{R}s_0 \cdots s_N\mathtt{l} < \mathtt{R}s_0 \cdots s_N < \mathtt{R}s_0 \cdots s_N\mathtt{r}.$$

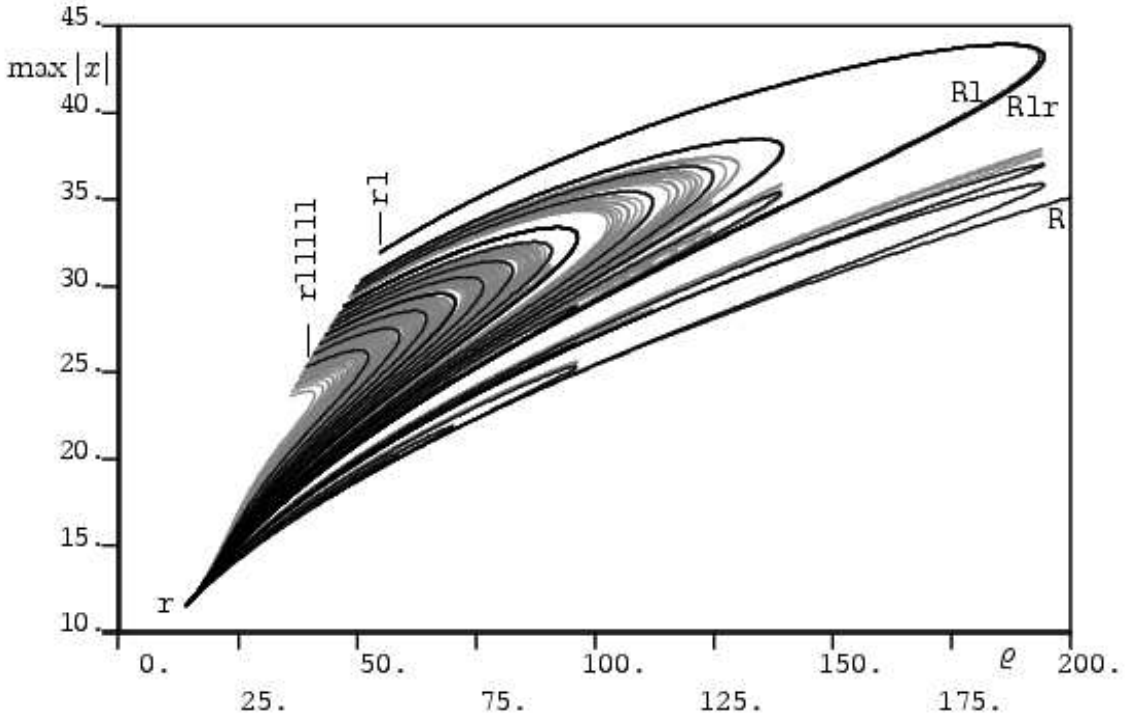

Figure 11. All computed curves of heteroclinic orbits `R*` up to level 8, shown as the maximum of $|x|$ over the heteroclicic orbit versus ϱ; the curves up to level 4 are highlighted in black. All curves emanate from the homoclinic explosion point at $\varrho_{\mathtt{r}} \approx 13.9265$. With the exception of curve `R`, all curves have folds and end at co-dimension-one homoclinic orbits of the origin. For example, curve `Rl` ends at the homoclinic orbits `rl`, while curve `Rlr` ends at `lr`, which is the co-existing symmetric counterpart for the same ϱ-value. For level 4 the limiting homoclinic orbit with the lowest ϱ-value is `rllll`; see also figure 15 and figure 16.

In other words, the ordering (3) can be obtained by projecting all nodes of the binary tree onto a line, which corresponds in figure 9 to projection onto the r_0 axis. Due to symmetry, we have that $\mathtt{L}s_0 \cdots s_N$ has the same place in the ordering as its symmetric counterpart $\mathtt{R}\overline{s}_0 \cdots \overline{s}_N$.

4. Continuation of heteroclinic orbits in ϱ

It is an immediate question what happens to the binary tree of heteroclinic orbits when one varies the parameter ϱ. The discussion in section 1 and figure 8 suggest that all heteroclinic orbits we found for $\varrho = 28.0$ are created in the homoclinic explosion at $\varrho_{\mathtt{r}} \approx 13.9265$. Hence, one would expect that the heteroclinic orbits can be followed for decreasing ϱ to this value. On the other hand, it is not so clear what happens to the structure of heteroclinic orbits when one increases ϱ.

To address these questions we started continuations from all 512 heteroclinic orbits

for $\varrho = 28.0$ for decreasing and increasing ϱ. This process was implemented by level, so that all 2^i heteroclinic branches of level i are computed by starting a single script. To start the continuation of a given heteroclinic orbit a Newton step was applied to the approximate orbit corresponding to the respective minimum in figure 9. This ensures that the projection boundary conditions near the origin are satisfied within a high numerical accuracy, that is, the orbit segment ends in $E^s(\mathbf{0})$ near $\mathbf{0}$. This orbit segment was then continued in ϱ, where the total integration time T is a free parameter.

The computation is performed in two runs, one for initially decreasing ϱ and one for initially increasing ϱ. In the former case we pass the Hopf bifurcation at $\varrho_H = \frac{470}{19}$. From then on the heteroclinic orbit is between the saddle periodic orbit Γ^+ and the origin. In the computation we continue the eigendirection and appropriate distance from p^+. For $\varrho < \varrho_H$ we approximate a direction in $E^u(\Gamma^+)$ by a direction in $E^u(p^+)$. We checked that this approximation is acceptable; due to the 'flat' nature of Γ^+ and $E^u(\Gamma^+)$ any small initial distance from $W^u(\Gamma^+)$ decays after at most two revolutions around Γ^+ to below the accuracy of the computation. Therefore, simply by following the same boundary value setup through the Hopf bifurcation we obtain a smooth continuation process that then follows the homoclinic orbit from Γ^+ to $\mathbf{0}$. This procedure is numerically stable and stops (at the basic homoclinic explosion point $\varrho_{\mathtt{r}}$) when the total integration time T reaches a prespecified bound. Due to the required high accuracy, with a necessarily fine mesh of up to 4801 mesh points (AUTO constants NTST=1200 and NCOL=4), the overall amount of data thus created to represent the 512 solution branches is over 400Mb (before compression), while not even including all computed orbits.

Figure 11 shows all 512 branches of heteroclinic orbits up to level 8 in a plot of the maximum of $|x|$ over the heteroclinic orbit versus the parameter ϱ. To highlight the structure of this set the branches up to level 4 are shown in black, while those of higher levels are in gray. The overall result is that indeed all 512 branches emanate from the homoclinic explosion at $\varrho_{\mathtt{r}} \approx 13.9265$. As we have seen in figure 5, the periodic orbits $\Gamma^\pm$ approach the homoclinic orbits `r` and `l`, respectively, and this implies that all heteroclinic orbits in $W^u(\Gamma^\pm) \cup W^s(\mathbf{0})$ must do the same. This is illustrated in figure 12 for the examples of the heteroclinic orbits from figure 10 with symbolic sequences `rl` and `rlllr`.

When continued from the basic heteroclinic explosion point for increasing ϱ the heteroclinic orbit `R` continues on to infinity. All other branches of heteroclinic orbits have folds (LP points of `AUTO`) and then continue back to smaller values of ϱ. Each fold in Figure 11 represents a heteroclinic tangency between $W^u(p^+)$ and $W^s(\mathbf{0})$, where two intersection curves (with the same symbol sequence) come together and disappear as ϱ increases. As is apparent from figure 11, the intersection curves are lost in pairs one-by-one in heteroclinic tangencies until, for ϱ larger than about 194.6 the two-dimensional manifolds $W^u(p^+)$ and $W^s(\mathbf{0})$ intersect only in the curve `R`, which cannot be removed and remains as an intersection curve for all $\varrho > \varrho_{\mathtt{r}}$. Notice also that the folds accumulate at distinct ϱ-values and, in fact, many folds agree up to the first four digits of ϱ; see the full data in Appendix A. This is due to the fact that $W^u(p^+)$ contains many sheets

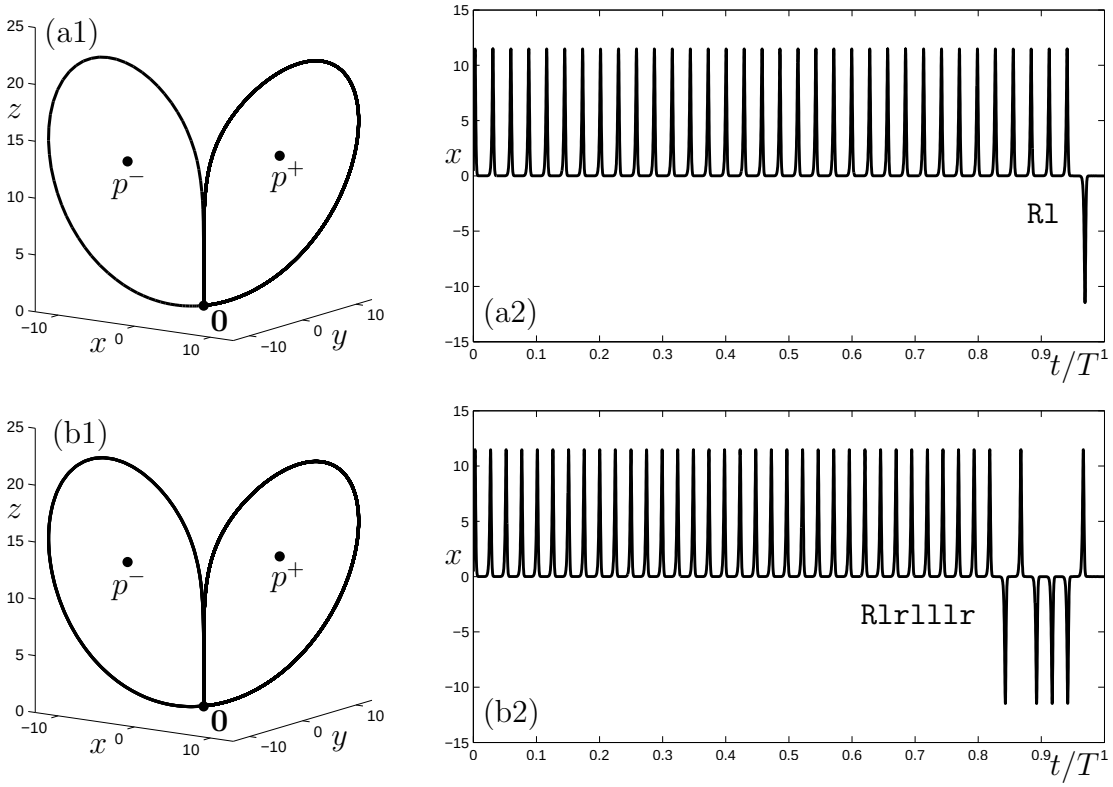

Figure 12. All branches of heteroclinic orbits emanate from the basic homoclinic explosion point at $\varrho_{\mathtt{r}} \approx 13.9265$. Shown is how the heteroclinic orbits from figure 10 with symbolic sequences `rl` (a) and `rlllr` (b), respectively, accumulate on the basic homoclinic orbit `r`; the limits are shown in phase space (left) and as time series of the x-value (right).

close to each other, which one-by-one have a tangency with $W^s(\mathbf{0})$ in a very small ϱ-interval. Indeed, this agrees with the notion that heteroclinic or homoclinic tangencies are typically accumulated by other tangencies [29].

Each branch of heteroclinic orbits, when continued from the basic homoclinic explosion at $\varrho_{\mathtt{r}}$ past its fold ends at a well-defined value of ϱ. For example, as is shown in figure 11, the heteroclinic orbits `Rl` and `Rlr` both end at $\varrho_{\mathtt{rl}} \approx 54.6460$. Note that all computed end points have ϱ-values larger than $\varrho = 28.0$. The left-most end point of any branch in level 4 is at $\varrho_{\mathtt{rllll}} \approx 39.1157$.

The obvious question is what characterizes the end points of the branches of heteroclinic orbits. In fact, each such end point is also a homoclinic explosion, that is, a homoclinic bifurcation of the origin just like that at $\varrho_{\mathtt{r}} \approx 13.9265$ but involving a more complicated pair of homoclinic orbits (and bifurcating periodic orbits). To define symbol sequences of these homoclinic orbits, note that the right branch of $W^u(\mathbf{0})$ at $\varrho_{\mathtt{r}} \approx 13.9265$ returns directly to $\mathbf{0}$ and we describe it with the symbol sequence `r` (hence, the naming of $\varrho_{\mathtt{r}}$). For $\varrho > \varrho_{\mathtt{r}}$ the right branch of the unstable manifold $W^u(\mathbf{0})$

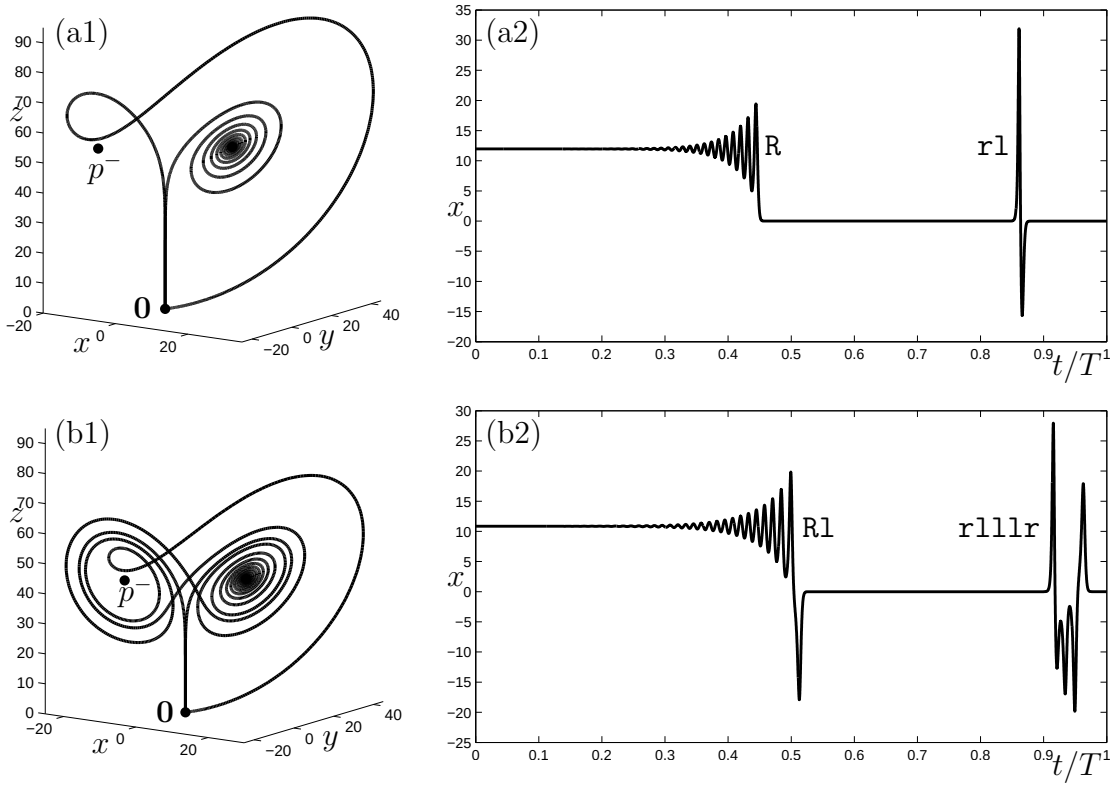

Figure 13. When followed in ϱ past the fold, the heteroclinic orbits from figure 10 limit on the homoclinic orbits with symbolic sequences `rl` (a) and `rlllr` (b), respectively; the limits are shown in phase space (left) and as time series of the x-value (right).

immediately crosses over to make at least one revolution around the left equilibrium p^-; see, for example, figure 5(a) and figure 2. Therefore, for all other homoclinic explosions the next symbol of its right homoclinic orbit is defined as $h_0 = \mathtt{l}$. The symbol sequence of the right homoclinic orbits is then defined as

$$\mathtt{rl}h_1 \cdots h_N, \quad \text{where} \begin{cases} h_j = \mathtt{l} & \text{if the } j\text{th revolution is around } p^-, \\ h_j = \mathtt{r} & \text{if the } j\text{th revolution is around } p^+. \end{cases}$$

Again, we refer to N as the level of the homoclinic orbit. By symmetry the left homoclinic orbit of the pair has the symbol sequence $\mathtt{lr}\overline{h}_1 \cdots \overline{h}_N$.

Figure 13 shows the limits of the heteroclinic orbits `Rl` and `Rlrlllr` of Figure 10 when continued in ϱ to their respective explosion points where they disappear. As the explosion point is approached, the heteroclinic orbit passes closer and closer near the origin. In the limit we obtain a heteroclinic orbit from p^+ to **0** folowed by a homoclinic orbit from **0** back to itself. How this homoclinic orbits 'splits off' can be seen in the time plots in the right column of figure 13. Notice that the heteroclinic orbit `Rl` ends at the homoclinic explosion `rl`, while `Rlrlllr` ends at the homoclinic explosion `rlllr`. In other words, in the former case an extra `r` is split off from the infinitely many revolutions

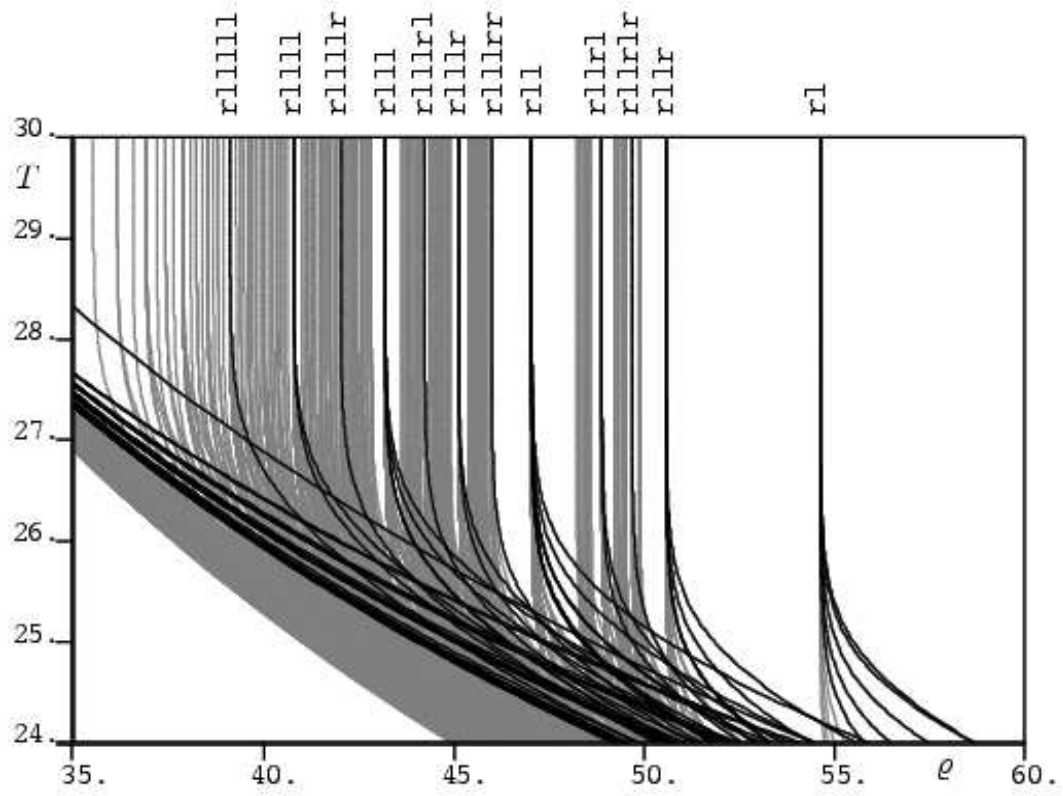

Figure 14. All computed curves of heteroclinic orbits (levels 0 to 8) in the plane of time T of the approximating orbit segment versus ϱ. Values of ϱ where T goes to infinity correspond to limiting co-dimension-one homoclinic orbits of the origin. For the heteroclinic orbits up to level 4 (black curves) the symbol sequences of the limiting homoclinic orbits (starting with `r`) are shown. Note that the symmetric counterparts of these homoclinic orbits co-exist for the same ϱ-values, and are the limits of some heteroclinic orbits; see also figure 15 and figure 16.

represented by `R`, while in the latter case the limiting homoclinic orbit consists of only a subpart of the symbolic sequence of the heteroclinic orbit `Rlrlllr`. Notice also that in figure 11, both `Rl` and `Rlr` end up at the same homoclinic explosion point labeled `rl`. However, `Rlr` has the symmetric counterpart `lr` as its limit.

5. Combinatorics of limiting homoclinic explosions

To determine which heteroclinic orbits end up at which homoclinic explosion points we extract automatically for each of the 512 branches of heteroclinic orbits the location of the fold, as well as the ϱ-value and symbol sequence of the limiting homoclinic orbit. This information is presented level by level in Appendix A and constitutes a major result of this paper. The key is that symbolic information is derived reliably on a large scale from numerical continuations of suitable orbit segments. We show now that this approach indeed allows for insight into the structure of how $W^s(\mathbf{0})$ interacts with $W^u(p^{\pm})$ and $W^u(\Gamma^{\pm})$ and, more generally, it reveals new aspects of how the dynamics

of the Lorenz system depends on ϱ.

In figure 14 we show all computed branches of heteroclinic orbits up to level 8 in the range $\varrho \in [35.0, 60.0]$. In contrast to figure 11, we now plot the integration time T of the approximating orbit segment. In this way, limiting codimension-one homoclinic orbits of the origin are made visible as points where T goes to infinity. All symbol sequences of the limiting homoclinic orbits for the black branches of heteroclinic orbits up to level 4 are shown at the top of figure 14. Note that we only show the symbol sequences starting with `r`, while some of the branches actually end up at the symmetric counterparts of these homoclinic orbits. Figure 14 clearly shows that many different branches of heteroclinic orbits end up at the same homoclinic explosion. Furthermore, not all possible symbol sequences of the binary tree up to level 4 (and up to level 8; see the data in Appendix A) appear as homoclinic orbits of explosion points.

To describe which homoclinic explosion points do occur we consider the recursive ordering of the the associated homoclinic orbits, which is defined exactly as in (3) where `R` is replaced by an initial `r`. Again, $\mathtt{l}h_0 \cdots h_N$ has the same place in the ordering as $\mathtt{r}\overline{h}_0 \cdots \overline{h}_N$.

Main results

(R1) For the heteroclinic orbit with symbol $\mathtt{R}s_0 \cdots s_N$ (recall that $s_0 = \mathtt{l}$) consider the smallest (with respect to the recursive ordering) of the $N+2$ subsequences $s_j \cdots s_N$ for $0 \le j \le N$ together with $\mathtt{r}s_0 \cdots s_N$. The corresponding branch of heteroclinic orbits ends at the homoclinic explosion point associated with the homoclinic orbit with this smallest symbol sequence; see figure 15.

(R2) As a consequence we find only those homoclinic explosion points as limits of heteroclinic orbits whose symbol $\mathtt{r}h_0 \cdots h_K$ (recall that $h_0 = \mathtt{l}$) (of the right homoclinic orbit) does not have a smaller subsequence, that is,

$$\mathtt{r}h_0 \cdots h_K < h_j \cdots h_K \quad \text{for all } 0 \le j \le K \tag{4}$$

We call these the homoclinic explosion points and associated homoclinic orbits *admissible*. The recursive ordering of the admissible homoclinic explosion points agrees with their ordering in terms of ϱ-values; see figure 16.

(R3) All branches of heteroclinic orbits that end up at the same homoclinic explosion point (that is, those that have a given symbol sequences $\mathtt{r}h_0 \cdots h_K$ or the symmetric counterpart $\mathtt{l}\overline{h}_0 \cdots \overline{h}_K$ as their smallest subsequence) have their folds at approximately the same value of ϱ; see figure 11.

Figure 15 illustrates (R1) with the binary tree of all heteroclinic orbits from p^+ to $\mathbf{0}$ up to level 5. The limiting homoclinic orbits are shown in boldface where colour indicates whether the first excursion is to the right or left, respectively. The reader may wish to check that the data in figure 15 indeed supports the criterion in (R1). Effectively, this tree illustates the many-to-one map from the full tree of heteroclinic orbits to the set of admissible homoclinic orbits.

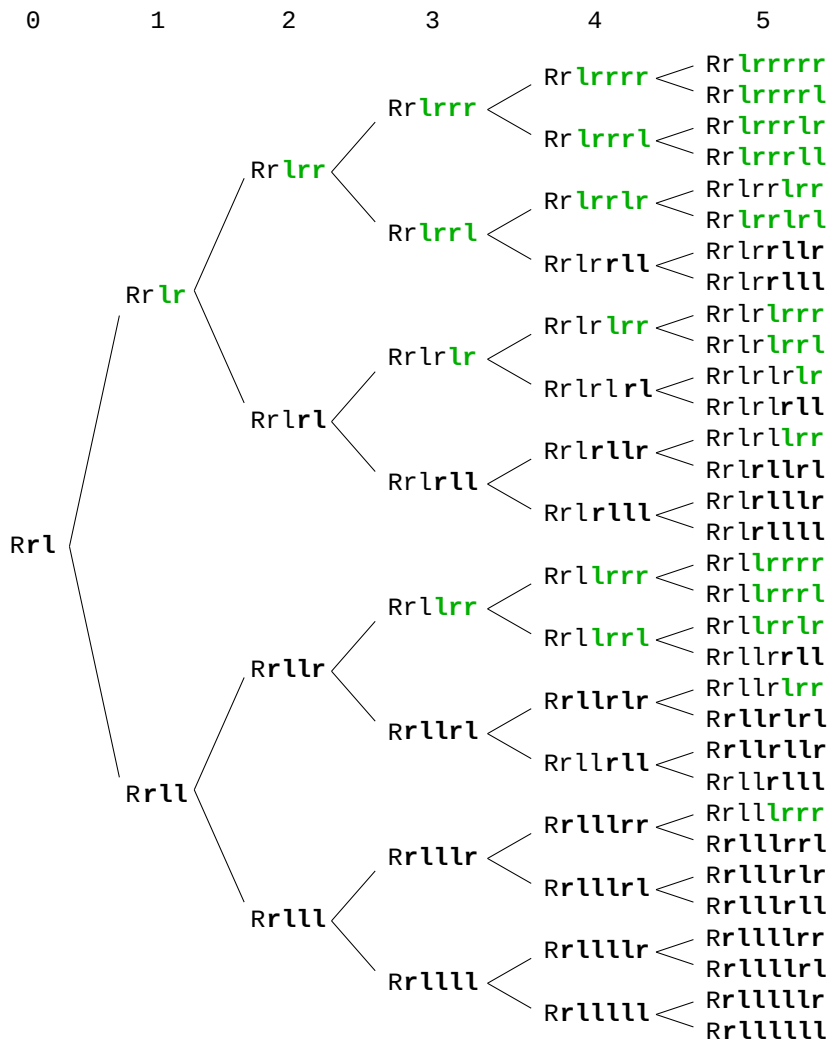

Figure 15. (Colour online) Tree up to level 5 of heteroclinic orbits from p^+ to $\mathbf{0}$ for $\varrho = 28.0$ (all symbols), and their limiting homoclinic orbits (boldface symbols) at the respective homoclinic explosion point. The colour/grayscale of boldface symbols distinguishes between homoclinic orbits that initially go to the left or to the right, respectively; the symmetric counterpart of any boldface symbol is the limit of the symmetrically related heteroclinic orbits from p^- to $\mathbf{0}$.

The admissible homoclinic orbits up to level 6 are shown boldface in the binary tree in figure 16 together with their ϱ-values as found in the continuation. Again, it can be checked that the admissible symbols satisfy the criterion given in (R2). Note that subtrees that do not contain any admissible homoclinic orbits have been left out of figure 16. For example, the entire subtree with root `rlr` does not contain any admissible homoclinic orbits.

Results (R1)-(R3) have been derived from and checked against the entire data in Appendix A. While this does not constitute a proof, this approach is similar to that of previous work on the symbolic dynamics of the Lorenz system — most notably that in

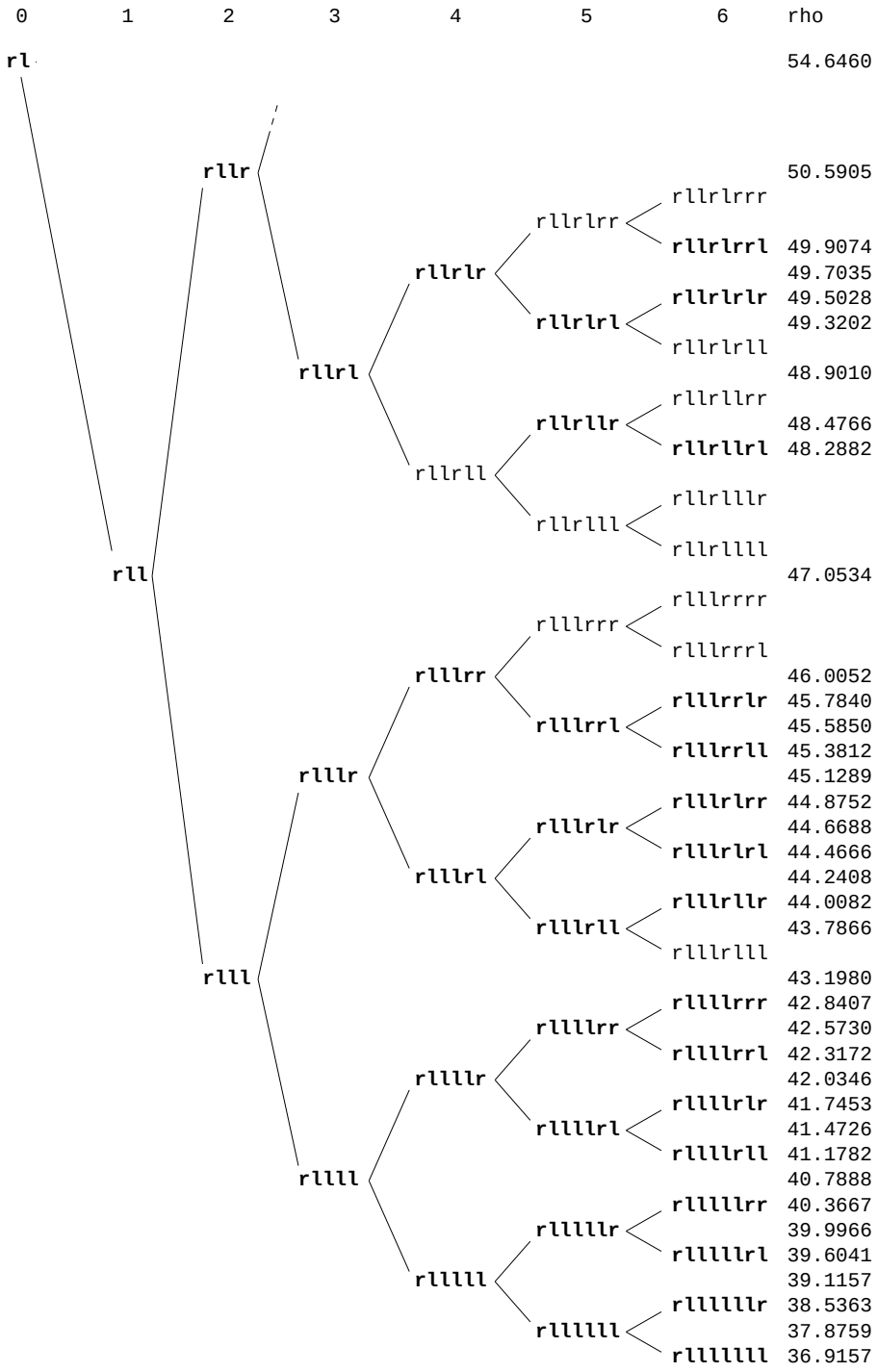

Figure 16. Tree of all admissible homoclinic explosion orbits (bold) up to level 6 and the ϱ-values of the respective homoclinic explosion points.

[33]. Note also that (R1)-(R3) are entirely in line with what one might expect from the knowledge of similar results for periodic orbits; see also section 6.

We remark that the admissible symbol sequences that we find as limits of heteroclinic orbits are exactly those that uniquely represent the homoclinic orbits in

which periodic orbits bifurcate in one-dimensional maps; see [33] and [17, Appendix A.1]. For example, the symbols symbol `rll`, `lrl` and `llr` describe the same periodic orbit when interpreted as an infinitely repeating itinerary. However, only `rll` is admissible as a homoclinic orbit, and also represents the itinerary of the bifurcating periodic orbit. Furthermore, admissible symbol sequences correspond to bifurcating periodic orbits of minimal period, which means that multiples of smaller periods are excluded as symbols.

All heteroclinic orbits that end in the same homoclinic explosion points are created in folds in a very narrow interval of ϱ-values. As was discussed in section 4, this is actually what one might expect in light of the multi-sheeted nature of $W^u(p^+)$: there are infinitely many tangencies with $W^s(\mathbf{0})$ with the different infinitely many sheets arbitrarily close together in ϱ; see also figure 3(c2). Indeed (R3) states that the final part of the symbol sequence is necessarily the same for all these orbits. In other words, these heteroclinic orbits only differ in their transient behaviour (of a well-defined symbolic type). In fact, these transients are very close together in the phase space of the Lorenz system. Nevertheless, our boundary value approach is perfectly able to distinguish them.

6. Discussion and open problems

We considered how the Lorenz manifold $W^s(\mathbf{0})$ and the unstable manifolds $W^u(p^\pm)$ and $W^u(\Gamma^\pm)$ of the secondary equilibria and bifurcating periodic orbits depend on the parameter ϱ. We computed these manifolds directly and also found and followed numerically their intersection curves, which are generic heteroclinic orbits between the origin and $p^\pm$ or $\Gamma^\pm$, respectively. Each homoclinic orbit is born in the basic well-known homoclinic explosion point at $\varrho_{\mathtt{r}} \approx 13.9265$ and was followed in ϱ past a fold to another homoclinic explosion point. We gave a self-consistent description of this scenario in terms of symbolic sequences of heteroclinic orbits and their limiting homoclinic explosion points. The basis for our results is the data set in Appendix A of automatically extracted symbolic information from continuations of the first 512 branches of heteroclinic orbits.

The symbolic dynamics of the generic heteroclinic and limiting homoclinic explosion points that we found is, by its nature, closely connected to the symbolic dynamics of periodic orbits that bifurcate in the homoclinic explosions. Indeed Sparrow [33, Chapter 5] presents a self-consistent scenario of how periodic orbits in the Lorenz attractor are created and destroyed as a function of ϱ in a combination of homoclinic explosions, period-doublings and T-point bifurcations. This is summarized in the bifurcation diagram [33, Fig. 5.12] and a list of homoclinic explosion points in [33, Appendix I]. While we computed many more homoclinic explosion points than Sparrow, we only find a subset of the explosion points for periodic orbits, namely the admissible ones as defined in result (R2). We do not find homoclinic explosion points (such as `rlrl`) that are due to period-doubled or symmetric periodic orbits, but the numerical ϱ-values in [33, Appendix I] of admissible explosion points agree with those in Appendix A. Also note that the admissible homoclinic explosion points we find all appear to be of 'type (a)' in the notation of Sparrow, which effectively means that the chaotic dynamics

i	hom-min	$\rho_{\min}(i)$	$\lvert\rho_{\min}(i)-\rho_{\min}(i-1)\rvert$	$\frac{\lvert\rho_{\min}(i-1)-\rho_{\min}(i-2)\rvert}{\lvert\rho_{\min}(i)-\rho_{\min}(i-1)\rvert}$
0	rl	5.4645952E+01		
1	rll	4.7053443E+01	7.592509	
2	rlll	4.3198042E+01	3.855401	1.96932
3	rllll	4.0788829E+01	2.409213	1.60027
4	rlllll	3.9115749E+01	1.673080	1.43999
5	rllllll	3.7875935E+01	1.239814	1.34946
6	rlllllll	3.6915667E+01	0.960268	1.29111
7	rllllllll	3.6147675E+01	0.767992	1.25036
8	rlllllllll	3.5518339E+01	0.629336	1.22032

Table 1. Convergence behaviour of $\rho_{\min}(i)$, the minimal ρ-value of any homoclinic orbit in level i.

they produce occurs for ϱ-values larger than that of the respective homoclinic explosion point.

The countable set of admissible homoclinic explosion points, which are due to the intersections of the underlying two-dimensional manifolds, can be interpreted as the backbone of the structure of all homoclinic explosion points. In order to bring out some general properties of this set we show in table 1 the admissible homoclinic explosion points $\mathtt{rl}^i$. According to result (R2), these have the smallest ϱ-value, denoted $\varrho_{\min}(i)$, of all homoclinic explosion points of level i. Notice that $\varrho_{\min}(i)$ decreases with i, so that the question arises what its limit is for $i \to \infty$. This limit cannot be derived from the data in table 1; the approximate convergence rate (last column) is far from constant. However, we can determine the limit of $\varrho_{\min}(i)$ with a topological argument. As ϱ is decreased towards the codimension-one heteroclinic bifurcation point $\varrho_{\rm het}$, the right branch of the one-dimensional unstable manifold $W^u(\mathbf{0})$ initially makes more and more turns around p^- and then (for $\varrho < \varrho_H \approx 24.7368$) around Γ^-; see also figure 2. Indeed, in the limit at $\varrho_{\rm het}$ it has the itinerary $\mathtt{rL}$. In other words, the limit of $\varrho_{\min}(i)$ for $i \to \infty$ is actually the codimension-one heteroclinic bifurcation point $\varrho_{\rm het} \approx 24.0579$. We conjecture that also the (accumulation points of) folds of the respective branches of generic heteroclinic orbits in result (R3) accumulate on $\varrho_{\rm het}$; see also figure 11.

The emerging self-consistent scenario is that $W^s(\mathbf{0}) \cap W^u(\Gamma^\pm)$ contains the entire binary tree of possible heteroclinic orbits for $\varrho \in (\varrho_{\mathtt{r}}, \varrho_{\rm het})$. In other words, there are no topological changes of $W^s(\mathbf{0}) \cap W^u(\Gamma^\pm)$ in this interval of 'pre-turbulence'. In contrast, for any fixed $\varrho > \varrho_{\rm het}$ already infinitely many topological changes have taken place. Namely, infinitely many extra heteroclinic orbits were created in admissible homoclinic explosion points and then lost in folds with the respective heteroclinic orbits born at $\varrho_{\mathtt{r}}$. One can determine which orbits are no longer present by considering the itinerary of the right branch of $W^u(\mathbf{0})$. As is shown in figure 17, for the classic value of $\varrho = 28.0$ it has the itinerary $\mathtt{rl}^{25}\mathtt{r}\cdots$, that is, it initially makes exactly 25 revolutions around p^- before returning back to near p^+. It is important to realize that the right branch of

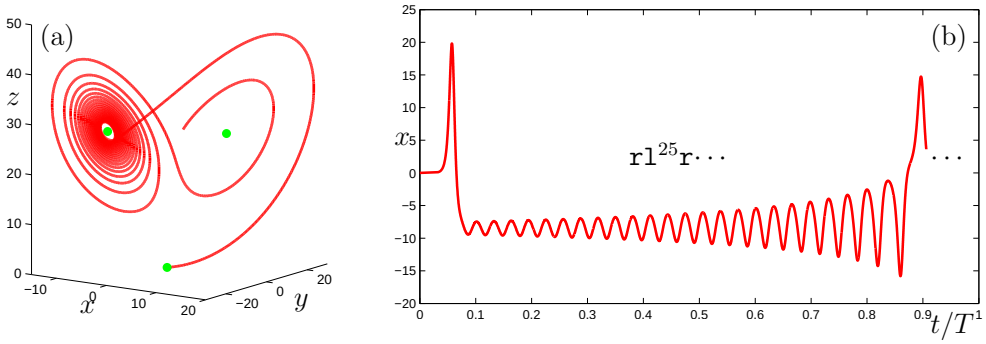

Figure 17. The itinerary of right branch of $W^u(\mathbf{0})$ for $\varrho = 28.0$ starts with $\mathtt{rl}^{25}\mathtt{r}\cdots$, which shows that the homoclinic explosion $\mathtt{rl}^{26}$ occurs for $\varrho < 28.0$.

$W^u(\mathbf{0})$, which forms the boundary of $W^u(p^+)$, constitutes the re-injection closest to p^-; see also figure 7(a). Therefore, after the initial infinitely many revolutions around p^+, any orbit on $W^u(p^+)$ may have at most this maximal number of 25 revolutions around p^- before the transition back to near p^+. By taking into account the symmetry, we can conclude that the limiting homoclinic explosion points of any branch of heteroclinic orbits with symbol sequences containing $\mathtt{l}^{26}$ or $\mathtt{r}^{26}$ as a subsequence occur for $\varrho < 28.0$. As was already noted in [33, Chapter 3.3], this has consequences for the periodic orbits in the Lorenz attractor: any periodic orbit for $\varrho = 28.0$ has at most 25 consecutive revolutions around p^- or p^+. (This corresponds to the fact that the orbit of (-1) under the associated one-dimensional map determines the topological equivalence class of the attractor [15, Chapter 6.4].) In particular, the longest periodic orbit of the form $\mathtt{rl}^i$ is that for $i = 25$. Note that, with his method, Viswanath [36] could only find these periodic orbits up to $\mathtt{rl}^{23}$; a reason for this may be that these periodic orbits pass closer and closer near the origing at i increases.

There are many avenues for future work. First of all, it is possible to consider the dependence of the Lorenz manifold $W^s(\mathbf{0})$ in relation to the unstable manifolds $W^u(p^\pm)$ and $W^u(\Gamma^\pm)$ with respect to the other parameters β and σ. Indeed the start data in figure 9 for the first 512 heteroclinic orbits can be used to follow the respective branches in β or σ. Furthermore, it would be an interesting and challenging project to start continuations of periodic orbits from (all of) the homoclinic explosion points in Appendix A. In this way, the sketched bifurcation diagram [33, Fig. 5.12] could be computed directly and expanded upon. What is more, the codimension-one bifurcations, namely the homoclinic explosion points and the folds of heteroclinic branches (that is, heteroclinic tangency bifurcations), as well as period-doubling and saddle-node bifurcations of periodic orbits, can be continued in two parameters. It is also possible to use homoclinic branch switching as implemented in [26] to find homoclinic bifurcations that are not part of our set of admissible homoclinic explosion points. The combination of these techniques would allow one to compute and check the conjectural bifurcation diagrams in the (β, ϱ)-plane in [33, Chapter 9], as well as the bifurcation

diagrams in the (ϱ, σ)-plane in [7].

Another interesting direction of research is to find and follow suitable orbit segments (see also [9]) that allow one to compute directly the intersection curves of relevant two-dimensional manifolds with a Poincaré section such as Σ_ϱ. This approach is much more stable than single shooting methods, and it enables one to consider changes of the manifold structure directly in the Poincaré section. This might provide useful information on the associated foliations, which in turn are relevant for the reduction of the Poincaré map to a one-dimensional map.

More generally, we hope that the results and methods presented here will stimulate the analysis of the invariant manifold structure in other systems, whether they are chaotic or not.

Acknowledgements

The authors thank Ale Jan Homburg for helpful discussion on the symbolic dynamics of the Lorenz system. E.J.D. acknowledges the hospitality and support of the Bristol Centre for Applied Nonlinear Mathematics, and B.K. and H.M.O. that of Concordia University during several research visits. The research of E.J.D. was partially supported by an NSERC (Canada) Discovery Grant, and that of B.K. and of H.M.O. was supported by Advanced Research Fellowship grants from the Engineering and Physical Sciences Research Council (EPSRC).

References

[1] Abraham R H and Shaw C D 1985 *Dynamics — the geometry of behavior, Part three: global behavior* (Santa Cruz: Aerial Press).

[2] Afrajmovich V S, Bykov V V and Sil'nikov L P 1977 The origin and structure of the Lorenz attractor. (Russian) *Dokl. Akad. Nauk SSSR* **234**(2) 336–339.

[3] Back A, Guckenheimer J, Myers M R, Wicklin F J and Worfolk P A 1992 DsTool: Computer assisted exploration of dynamical systems *Notices Amer. Math. Soc.* **39** 303–309.

[4] Doedel E J 1981 AUTO, a program for the automatic bifurcation analysis of autonomous systems *Congr. Numer.* **30** 265–384.

[5] Doedel E J, Champneys A R, Fairgrieve T F, Kuznetsov Yu A, Sandstede B and Wang X J 1997 AUTO97: Continuation and bifurcation software for ordinary differential equations (`http://indy.cs.concordia.ca/auto/main.html`).

[6] Doedel E J, Paffenroth R C, Champneys A R, Fairgrieve T F, Kuznetsov Yu A, Oldeman B E, Sandstede B and Wang X J 2000 AUTO2000: Continuation and bifurcation software for ordinary differential equations; available via (`http://cmvl.cs.concordia.ca/`).

[7] Dullin H R, Schmidt S, Richter P H and Grossmann S K 2006 Extended phase diagram of the Lorenz model *arXiv preprint nlin.CD/0504024* (`http://arxiv.org/abs/nlin.CD/0504024`).

[8] Eckhardt B and Ott G 1994 Periodic orbit analysis of the Lorenz attractor *Z. Phys.* B **93** 259–266.

[9] England J P, Krauskopf B and Osinga H M 2005 Computing one-dimensional global manifolds of Poincaré maps by continuation *SIAM J. Appl. Dynam. Syst.* **4**(4) 1008–1041.

[10] England J P, Krauskopf B and Osinga H M 2007 Computingtwo-dimensional global invariant manifolds in slow-fast systems *Int. J. Bifurcation and Chaos* **17**(3) (in press)

[11] Franceschini V, Gilberti C and Zheng Z 1993 Characterization of the Lorenz attractor by unstable periodic orbits *Nonlinearity* **6** 251–258.

[12] Ghrist R, Holmes P J and Sullivan M C 1997 *Knots and links in three-dimensional flows* Lecture Notes in Mathematics **1654** (Berlin: Springer-Verlag).

[13] Gilmore R and Lefranc M 2004 *The topology of chaos: Alice in stretch and squeezeland* (New York: Wiley-Interscience)

[14] Glendinning P and Sparrow C 1984 Local and global behavior near homoclinic orbits *J. Statist. Phys.* **35**(5/6) 645–696.

[15] Guckenheimer J and Holmes P 1986 *Nonlinear Oscillations Dynamical Systems and Bifurcations of Vector Fields* Second Printing (New York: Springer-Verlag).

[16] Guckenheimer J and Williams R 1979 Structural stability of Lorenz attractors *Publ. Math. IHES* **50** 59–72.

[17] Homburg A J and Krauskopf B 2000 Resonant homoclinic flip bifurcations *J. Dyn. Diff. Eqs.* **12**(4) 807–850.

[18] Kaplan J L and Yorke J A 1979 Preturbulence, a regine observed in a fluid flow model of Lorenz *Comm. Math. Phys.* **67** 93–108.

[19] Krauskopf B and Osinga H M 1999 Two-dimensional global manifolds of vector fields *Chaos* **9**(3) 768–774.

[20] Krauskopf B and Osinga H M 2003 Computing geodesic level sets on global (un)stable manifolds of vector fields *SIAM J. Appl. Dyn. Sys.* **4**(2) 546–569.

[21] Krauskopf B and Osinga H M 2004 The Lorenz manifold as a collection of geodesic level sets *Nonlinearity* **17**(1) C1–C6.

[22] Krauskopf B, Osinga H M, Doedel E J, Henderson M E, Guckenheimer J, Vladimirsky A, Dellnitz M and Junge O 2005 A survey of methods for computing (un)stable manifolds of vector fields *Int. J. Bifurcation and Chaos* **15**(3) 763-791.

[23] Kuznetsov Yu A 1995 *Elements of Applied Bifurcation Theory* Applied Mathematical Sciences **112** (New York: Springer-Verlag).

[24] Lorenz E N 1963 Deterministic nonperiodic flows *J. Atmospheric Sci.* **20** 130–141.

[25] Luzzatto S, Melbourne I and Paccaut F 2005 The Lorenz attractor is mixing *Comm. Math. Phys.* **260**(2) 393–401.
[26] Oldeman B E, Champneys A R and Krauskopf B 2003 Homoclinic branch switching: a numerical implementation of Lin's method *Int. J. Bifurcation and Chaos* **13**(10) 2977–2999.
[27] Osinga H M and Krauskopf B 2002 Visualizing the structure of chaos in the Lorenz system *Computers and Graphics* **26**(5) 815–823.
[28] Osinga H M and Krauskopf B 2004 Crocheting the Lorenz manifold *Math. Intelligencer* **26**(4) 25–37.
[29] Palis J and Takens F 1995 *Hyperbolicity and Sensitive Chaotic Dynamics at Homoclinic Bifurcations* (Cambridge: Cambridge University Press).
[30] Perelló C 1979 Intertwining invariant manifolds and Lorenz attractor in *Global theory of dynamical systems (Proc. Internat. Conf., Northwestern Univ., Evanston, Ill., 1979)*, Lecture Notes in Math. **819**, (Berlin: Springer-Verlag) pp. 375–378.
[31] Rand D 1978 The topological classification of Lorenz attractors *Math. Proc. Cambridge Philos. Soc.*. **83** 451–460.
[32] Robbins K 1979 Periodic solutions and bifurcation structure at high r in the Lorenz model at $\sigma = 10$ *SIAM J. Appl. Math.* **36** 457–472.
[33] Sparrow C 1982 *The Lorenz Equations: Bifurcations, Chaos and Strange Attractors*, Appl. Math. Sci. No. 41 (New York: Springer-Verlag).
[34] Tucker W 1999 The Lorenz attractor exists *Comptes Rendus de l'Académie des Scienes Série I. Mathématique* **328**(12) 1197–1202.
[35] Viana M 2000 What's new on Lorenz strange attractors? *Math. Intelligencer* **22**(3) 6–19.
[36] Viswanath D 2003 Symbolic dynamics and periodic orbits if the Lorenz attractor *Nonlinearity* **16**(3) 1035–1056.
[37] Williams R F 1979 The structure of Lorenz attractors *Publ. Math. IHES* **50** 101–152.
[38] Williams R F 1998 The universal templates of Ghrist *Bull. AMS* **35**(2) 145–156.

Appendix A. Table of heteroclinic orbit data

lev-#	Het	Hom	rho-limit	LP
0-000	Rl	rl	5.4645952E+01	1.937E+02
1-000	Rlr	lr	5.4645952E+01	1.946E+02
1-001	Rll	rll	4.7053443E+01	9.648E+01
2-000	Rlrr	lrr	4.7053443E+01	9.650E+01
2-001	Rlrl	rl	5.4645952E+01	1.946E+02
2-002	Rllr	rllr	5.0590467E+01	1.395E+02
2-003	Rlll	rlll	4.3198042E+01	7.064E+01
3-000	Rlrrr	lrrr	4.3198042E+01	7.064E+01
3-001	Rlrrl	lrrl	5.0590467E+01	1.397E+02
3-002	Rlrlr	lr	5.4645952E+01	1.946E+02
3-003	Rlrll	rll	4.7053443E+01	9.650E+01
3-004	Rllrr	lrr	4.7053443E+01	9.648E+01
3-005	Rllrl	rllrl	4.8900976E+01	1.123E+02
3-006	Rlllr	rlllr	4.5128887E+01	8.272E+01
3-007	Rllll	rllll	4.0788829E+01	5.898E+01

lev-#	Het	Hom	rho-limit	LP
4-000	Rlrrrr	lrrrr	4.0788829E+01	5.898E+01
4-001	Rlrrrl	lrrrl	4.5128887E+01	8.273E+01
4-002	Rlrrlr	lrrlr	4.8900976E+01	1.123E+02
4-003	Rlrrll	rll	4.7053443E+01	9.648E+01
4-004	Rlrlrr	lrr	4.7053443E+01	9.650E+01
4-005	Rlrlrl	rl	5.4645952E+01	1.946E+02
4-006	Rlrllr	rllr	5.0590467E+01	1.397E+02
4-007	Rlrlll	rlll	4.3198042E+01	7.064E+01
4-008	Rllrrr	lrrr	4.3198042E+01	7.064E+01
4-009	Rllrrl	lrrl	5.0590467E+01	1.395E+02
4-010	Rllrlr	rllrlr	4.9703500E+01	1.249E+02
4-011	Rllrll	rll	4.7053443E+01	9.650E+01
4-012	Rlllrr	rlllrr	4.6005196E+01	9.095E+01
4-013	Rlllrl	rlllrl	4.4240808E+01	7.656E+01
4-014	Rllllr	rllllr	4.2034581E+01	6.473E+01
4-015	Rllllll	rllllll	3.9115749E+01	5.235E+01

lev-#	Het	Hom	rho-limit	LP
5-000	Rlrrrrr	lrrrrr	3.9115749E+01	5.235E+01
5-001	Rlrrrrl	lrrrrl	4.2034581E+01	6.473E+01
5-002	Rlrrrlr	lrrrlr	4.4240808E+01	7.657E+01
5-003	Rlrrrll	lrrrll	4.6005196E+01	9.097E+01
5-004	Rlrrlrr	lrr	4.7053443E+01	9.650E+01
5-005	Rlrrlrl	lrrlrl	4.9703500E+01	1.250E+02
5-006	Rlrrllr	rllr	5.0590467E+01	1.395E+02
5-007	Rlrrlll	rlll	4.3198042E+01	7.064E+01
5-008	Rlrlrrr	lrrr	4.3198042E+01	7.064E+01
5-009	Rlrlrrl	lrrl	5.0590467E+01	1.397E+02
5-010	Rlrlrlr	lr	5.4645952E+01	1.946E+02
5-011	Rlrlrll	rll	4.7053443E+01	9.650E+01
5-012	Rlrllrr	lrr	4.7053443E+01	9.648E+01
5-013	Rlrllrl	rllrl	4.8900976E+01	1.123E+02
5-014	Rlrlllr	rlllr	4.5128887E+01	8.273E+01
5-015	Rlrllll	rllll	4.0788829E+01	5.898E+01
5-016	Rllrrrr	lrrrr	4.0788829E+01	5.898E+01
5-017	Rllrrrl	lrrrl	4.5128887E+01	8.272E+01
5-018	Rllrrlr	lrrlr	4.8900976E+01	1.123E+02
5-019	Rllrrll	rll	4.7053443E+01	9.648E+01
5-020	Rllrlrr	lrr	4.7053443E+01	9.650E+01
5-021	Rllrlrl	rllrlrl	4.9320171E+01	1.175E+02
5-022	Rllrllr	rllrllr	4.8476611E+01	1.072E+02
5-023	Rllrlll	rlll	4.3198042E+01	7.064E+01
5-024	Rlllrrr	lrrr	4.3198042E+01	7.064E+01
5-025	Rlllrrl	rlllrrl	4.5585034E+01	8.619E+01
5-026	Rlllrlr	rlllrlr	4.4668849E+01	7.953E+01
5-027	Rlllrll	rlllrll	4.3786551E+01	7.358E+01
5-028	Rllllrr	rllllrr	4.2573041E+01	6.758E+01
5-029	Rllllrl	rllllrl	4.1472638E+01	6.200E+01
5-030	Rllllll	rllllll	3.9996627E+01	5.573E+01
5-031	Rllllll	rllllll	3.7875935E+01	4.807E+01

lev-#	Het	Hom	rho-limit	LP
6-000	Rlrrrrrr	lrrrrrr	3.7875935E+01	4.807E+01
6-001	Rlrrrrrl	lrrrrrl	3.9996627E+01	5.573E+01
6-002	Rlrrrrlr	lrrrrlr	4.1472638E+01	6.200E+01
6-003	Rlrrrrll	lrrrrll	4.2573041E+01	6.758E+01
6-004	Rlrrrlrr	lrrrlrr	4.3786551E+01	7.359E+01

6-005	Rlrrrlrl	lrrrlrl	4.4668849E+01	7.954E+01
6-006	Rlrrrllr	lrrrllr	4.5585034E+01	8.620E+01
6-007	Rlrrrlll	rlll	4.3198042E+01	7.064E+01
6-008	Rlrrlrrr	lrrr	4.3198042E+01	7.063E+01
6-009	Rlrrlrrl	lrrlrrl	4.8476611E+01	1.072E+02
6-010	Rlrrlrlr	lrrlrlr	4.9320171E+01	1.176E+02
6-011	Rlrrlrll	rll	4.7053443E+01	9.650E+01
6-012	Rlrrllrr	lrr	4.7053443E+01	9.648E+01
6-013	Rlrrllrl	rllrl	4.8900976E+01	1.123E+02
6-014	Rlrrlllr	rllllr	4.5128887E+01	8.272E+01
6-015	Rlrrllll	rllll	4.0788829E+01	5.898E+01
6-016	Rlrlrrrr	lrrrr	4.0788829E+01	5.898E+01
6-017	Rlrlrrrl	lrrrl	4.5128887E+01	8.273E+01
6-018	Rlrlrrlr	lrrlr	4.8900976E+01	1.123E+02
6-019	Rlrlrrll	rll	4.7053443E+01	9.648E+01
6-020	Rlrlrlrr	lrr	4.7053443E+01	9.650E+01
6-021	Rlrlrlrl	rl	5.4645952E+01	1.946E+02
6-022	Rlrlrllr	rllr	5.0590467E+01	1.397E+02
6-023	Rlrlrlll	rlll	4.3198042E+01	7.064E+01
6-024	Rlrllrrr	lrrr	4.3198042E+01	7.064E+01
6-025	Rlrllrrl	lrrl	5.0590467E+01	1.395E+02
6-026	Rlrllrrl	rllrlr	4.9703500E+01	1.250E+02
6-027	Rlrllrll	rll	4.7053443E+01	9.650E+01
6-028	Rlrlllrr	rlllrr	4.6005196E+01	9.097E+01
6-029	Rlrlllrl	rlllrl	4.4240808E+01	7.657E+01
6-030	Rlrllllr	rllllr	4.2034581E+01	6.473E+01
6-031	Rlrlllll	rlllll	3.9115749E+01	5.235E+01
6-032	Rllrrrrr	lrrrrr	3.9115749E+01	5.235E+01
6-033	Rllrrrrl	lrrrrl	4.2034581E+01	6.473E+01
6-034	Rllrrrlr	lrrrlr	4.4240808E+01	7.656E+01
6-035	Rllrrrll	lrrrll	4.6005196E+01	9.095E+01
6-036	Rllrrlrr	lrr	4.7053443E+01	9.650E+01
6-037	Rllrrlrl	lrrlrl	4.9703500E+01	1.249E+02
6-038	Rllrrllr	rllr	5.0590467E+01	1.395E+02
6-039	Rllrrlll	rlll	4.3198042E+01	7.064E+01
6-040	Rllrlrrr	lrrr	4.3198042E+01	7.064E+01
6-041	Rllrlrrl	rllrlrrl	4.9907384E+01	1.302E+02
6-042	Rllrlrlr	rllrlrlr	4.9502803E+01	1.213E+02
6-043	Rllrlrll	rll	4.7053443E+01	9.650E+01
6-044	Rllrllrr	lrr	4.7053443E+01	9.648E+01
6-045	Rllrllrl	rllrllrl	4.8288164E+01	1.039E+02
6-046	Rllrlllr	rllllr	4.5128887E+01	8.273E+01

6-047	Rllrllll	rllll	4.0788829E+01	5.898E+01
6-048	Rlllrrrr	lrrrr	4.0788829E+01	5.898E+01
6-049	Rlllrrrl	lrrrl	4.5128887E+01	8.272E+01
6-050	Rlllrrlr	rlllrrlr	4.5783995E+01	8.824E+01
6-051	Rlllrrll	rlllrrll	4.5381239E+01	8.421E+01
6-052	Rlllrlrr	rlllrlrr	4.4875194E+01	8.122E+01
6-053	Rlllrlrl	rlllrlrl	4.4466583E+01	7.805E+01
6-054	Rlllrllr	rlllrllr	4.4008209E+01	7.508E+01
6-055	Rlllrlll	rlll	4.3198042E+01	7.064E+01
6-056	Rllllrrr	rllllrrr	4.2840715E+01	6.950E+01
6-057	Rllllrrl	rllllrrl	4.2317190E+01	6.616E+01
6-058	Rllllrlr	rllllrlr	4.1745287E+01	6.332E+01
6-059	Rllllrll	rllllrll	4.1178183E+01	6.062E+01
6-060	Rlllllrr	rlllllrr	4.0366729E+01	5.726E+01
6-061	Rlllllrl	rlllllrl	3.9604078E+01	5.418E+01
6-062	Rllllllr	rllllllr	3.8536284E+01	5.030E+01
6-063	Rlllllll	rlllllll	3.6915667E+01	4.507E+01

lev-#	Het	Hom	rho-limit	LP
7-000	Rlrrrrrrr	lrrrrrrr	3.6915667E+01	4.507E+01
7-001	Rlrrrrrrl	lrrrrrrl	3.8536284E+01	5.030E+01
7-002	Rlrrrrrlr	lrrrrrlr	3.9604078E+01	5.418E+01
7-003	Rlrrrrrll	lrrrrrll	4.0366729E+01	5.726E+01
7-004	Rlrrrrlrr	lrrrrlrr	4.1178183E+01	6.062E+01
7-005	Rlrrrrlrl	lrrrrlrl	4.1745287E+01	6.332E+01
7-006	Rlrrrrllr	lrrrrllr	4.2317190E+01	6.616E+01
7-007	Rlrrrrlll	lrrrrlll	4.2840715E+01	6.950E+01
7-008	Rlrrrlrrr	lrrr	4.3198042E+01	7.064E+01
7-009	Rlrrrlrrl	lrrrlrrl	4.4008209E+01	7.508E+01
7-010	Rlrrrlrlr	lrrrlrlr	4.4466583E+01	7.805E+01
7-011	Rlrrrlrll	lrrrlrll	4.4875194E+01	8.122E+01
7-012	Rlrrrllrr	lrrrllrr	4.5381239E+01	8.422E+01
7-013	Rlrrrllrl	lrrrllrl	4.5783995E+01	8.825E+01
7-014	Rlrrrlllr	rllllr	4.5128887E+01	8.272E+01
7-015	Rlrrrllll	rllll	4.0788829E+01	5.898E+01
7-016	Rlrrlrrrr	lrrrr	4.0788829E+01	5.898E+01
7-017	Rlrrlrrrl	lrrrl	4.5128887E+01	8.273E+01
7-018	Rlrrlrrlr	lrrlrrlr	4.8288164E+01	1.039E+02
7-019	Rlrrlrrll	rll	4.7053443E+01	9.648E+01
7-020	Rlrrlrlrr	lrr	4.7053443E+01	9.650E+01
7-021	Rlrrlrlrl	lrrlrlrl	4.9502803E+01	1.214E+02

7-022	Rlrrlrllr	lrrlrllr	4.9907384E+01	1.303E+02
7-023	Rlrrlrlll	rlll	4.3198042E+01	7.064E+01
7-024	Rlrrllrrr	lrrr	4.3198042E+01	7.064E+01
7-025	Rlrrllrrl	lrrl	5.0590467E+01	1.395E+02
7-026	Rlrrllrlr	rllrlr	4.9703500E+01	1.249E+02
7-027	Rlrrllrll	rll	4.7053443E+01	9.650E+01
7-028	Rlrrlllrr	rlllrr	4.6005196E+01	9.095E+01
7-029	Rlrrlllrl	rlllrl	4.4240808E+01	7.656E+01
7-030	Rlrrllllr	rllllr	4.2034581E+01	6.473E+01
7-031	Rlrrllllll	rllllll	3.9115749E+01	5.235E+01
7-032	Rlrlrrrrr	lrrrrr	3.9115749E+01	5.235E+01
7-033	Rlrlrrrrl	lrrrrl	4.2034581E+01	6.473E+01
7-034	Rlrlrrrlr	lrrrlr	4.4240808E+01	7.657E+01
7-035	Rlrlrrrll	lrrrll	4.6005196E+01	9.097E+01
7-036	Rlrlrrlrr	lrr	4.7053443E+01	9.650E+01
7-037	Rlrlrrlrl	lrrlrl	4.9703500E+01	1.250E+02
7-038	Rlrlrrllr	rllr	5.0590467E+01	1.395E+02
7-039	Rlrlrrlll	rlll	4.3198042E+01	7.064E+01
7-040	Rlrlrlrrr	lrrr	4.3198042E+01	7.064E+01
7-041	Rlrlrlrrl	lrrl	5.0590467E+01	1.397E+02
7-042	Rlrlrlrlr	lr	5.4645952E+01	1.946E+02
7-043	Rlrlrlrll	rll	4.7053443E+01	9.650E+01
7-044	Rlrlrllrr	lrr	4.7053443E+01	9.648E+01
7-045	Rlrlrllrl	rllrl	4.8900976E+01	1.123E+02
7-046	Rlrlrlllr	rlllr	4.5128887E+01	8.270E+01
7-047	Rlrlrllll	rllll	4.0788829E+01	5.898E+01
7-048	Rlrlllrrr	lrrrr	4.0788829E+01	5.898E+01
7-049	Rlrlllrrl	lrrrl	4.5128887E+01	8.272E+01
7-050	Rlrlllrlr	lrrlr	4.8900976E+01	1.123E+02
7-051	Rlrlllrll	rll	4.7053443E+01	9.648E+01
7-052	Rlrllrrlr	lrr	4.7053443E+01	9.650E+01
7-053	Rlrllrrll	rllrlrl	4.9320171E+01	1.176E+02
7-054	Rlrllrllr	rllrllr	4.8476611E+01	1.072E+02
7-055	Rlrllrlll	rlll	4.3198042E+01	7.064E+01
7-056	Rlrlllrrr	lrrr	4.3198042E+01	7.064E+01
7-057	Rlrlllrrl	rlllrrl	4.5585034E+01	8.620E+01
7-058	Rlrlllrlr	rlllrlr	4.4668849E+01	7.954E+01
7-059	Rlrlllrll	rlllrll	4.3786551E+01	7.359E+01
7-060	Rlrllllrr	rllllrr	4.2573041E+01	6.758E+01
7-061	Rlrllllrl	rllllrl	4.1472638E+01	6.200E+01
7-062	Rlrlllllr	rllllllr	3.9996627E+01	5.573E+01
7-063	Rlrlllllll	rlllllll	3.7875935E+01	4.807E+01

7-064	Rllrrrrrr	lrrrrrr	3.7875935E+01	4.807E+01
7-065	Rllrrrrrl	lrrrrrl	3.9996627E+01	5.573E+01
7-066	Rllrrrrlr	lrrrrlr	4.1472638E+01	6.200E+01
7-067	Rllrrrrll	lrrrrll	4.2573041E+01	6.758E+01
7-068	Rllrrrlrr	lrrrlrr	4.3786551E+01	7.358E+01
7-069	Rllrrrlrl	lrrrlrl	4.4668849E+01	7.953E+01
7-070	Rllrrrllr	lrrrllr	4.5585034E+01	8.619E+01
7-071	Rllrrrlll	rlll	4.3198042E+01	7.064E+01
7-072	Rllrrlrrr	lrrr	4.3198042E+01	7.064E+01
7-073	Rllrrlrrl	lrrlrrl	4.8476611E+01	1.072E+02
7-074	Rllrrlrlr	lrrlrlr	4.9320171E+01	1.175E+02
7-075	Rllrrlrll	rll	4.7053443E+01	9.650E+01
7-076	Rllrrllrr	lrr	4.7053443E+01	9.648E+01
7-077	Rllrrllrl	rllrl	4.8900976E+01	1.123E+02
7-078	Rllrrlllr	rllllr	4.5128887E+01	8.272E+01
7-079	Rllrrllll	rllll	4.0788829E+01	5.898E+01
7-080	Rllrlrrrr	lrrrr	4.0788829E+01	5.898E+01
7-081	Rllrlrrlr	lrrrl	4.5128887E+01	8.273E+01
7-082	Rllrlrrlr	lrrlr	4.8900976E+01	1.123E+02
7-083	Rllrlrrll	rll	4.7053443E+01	9.648E+01
7-084	Rllrlrlrr	lrr	4.7053443E+01	9.649E+01
7-085	Rllrlrlrl	rllrlrlrl	4.9415660E+01	1.192E+02
7-086	Rllrlrllr	rllrlrllr	4.9223448E+01	1.157E+02
7-087	Rllrlrlll	rlll	4.3198042E+01	7.064E+01
7-088	Rllrllrrr	lrrr	4.3198042E+01	7.064E+01
7-089	Rllrllrrl	rllrllrrl	4.8575486E+01	1.088E+02
7-090	Rllrllrlr	rllrllrlr	4.8378349E+01	1.057E+02
7-091	Rllrllrll	rll	4.7053443E+01	9.650E+01
7-092	Rllrlllrr	rlllrr	4.6005196E+01	9.097E+01
7-093	Rllrlllrl	rlllrl	4.4240808E+01	7.657E+01
7-094	Rllrllllr	rllllr	4.2034581E+01	6.473E+01
7-095	Rllrlllll	rlllll	3.9115749E+01	5.235E+01
7-096	Rlllrrrrr	lrrrrr	3.9115749E+01	5.235E+01
7-097	Rlllrrrrl	lrrrrl	4.2034581E+01	6.473E+01
7-098	Rlllrrrlr	lrrrlr	4.4240808E+01	7.656E+01
7-099	Rlllrrrll	lrrrll	4.6005196E+01	9.095E+01
7-100	Rlllrrlrr	rlllrrlrr	4.5882296E+01	8.969E+01
7-101	Rlllrrlrl	rlllrrlrl	4.5689098E+01	8.716E+01
7-102	Rlllrrllr	rlllrrllr	4.5479793E+01	8.524E+01
7-103	Rlllrrlll	rlll	4.3198042E+01	7.064E+01
7-104	Rlllrlrrr	lrrr	4.3198042E+01	7.064E+01
7-105	Rlllrlrrl	rlllrlrrl	4.4775570E+01	8.033E+01

7-106	Rlllrlrlr	rlllrlrlr	4.4563090E+01	7.877E+01
7-107	Rlllrlrll	rlllrlrll	4.4366435E+01	7.728E+01
7-108	Rlllrllrr	rlllrllrr	4.4113118E+01	7.584E+01
7-109	Rlllrllrl	rlllrllrl	4.3904242E+01	7.435E+01
7-110	Rlllrlllr	rlllrlllr	4.3663185E+01	7.273E+01
7-111	Rlllrllll	rllll	4.0788829E+01	5.898E+01
7-112	Rllllrrrr	lrrrr	4.0788829E+01	5.898E+01
7-113	Rllllrrrl	rllllrrrl	4.2710418E+01	6.840E+01
7-114	Rllllrrlr	rllllrrlr	4.2438623E+01	6.684E+01
7-115	Rllllrrll	rllllrrll	4.2191696E+01	6.548E+01
7-116	Rllllrlrr	rllllrlrr	4.1875364E+01	6.399E+01
7-117	Rllllrlrl	rllllrlrl	4.1617139E+01	6.268E+01
7-118	Rllllrllr	rllllrllr	4.1322385E+01	6.130E+01
7-119	Rllllrlll	rllllrlll	4.1018158E+01	5.986E+01
7-120	Rllllllrrr	rllllllrrr	4.0548574E+01	5.806E+01
7-121	Rllllllrrl	rllllllrrl	4.0191753E+01	5.652E+01
7-122	Rllllllrlr	rllllllrlr	3.9795226E+01	5.493E+01
7-123	Rllllllrll	rllllllrll	3.9395336E+01	5.337E+01
7-124	Rlllllllrr	rlllllllrr	3.8808602E+01	5.126E+01
7-125	Rlllllllrl	rlllllllrl	3.8244501E+01	4.929E+01
7-126	Rllllllllr	rllllllllr	3.7431219E+01	4.666E+01
7-127	Rlllllllll	rlllllllll	3.6147675E+01	4.285E+01

lev-#	Het	Hom	rho-limit	LP
8-000	Rlrrrrrrrr	lrrrrrrrr	3.6147675E+01	4.285E+01
8-001	Rlrrrrrrrl	lrrrrrrrl	3.7431219E+01	4.666E+01
8-002	Rlrrrrrrlr	lrrrrrrlr	3.8244501E+01	4.929E+01
8-003	Rlrrrrrrll	lrrrrrrll	3.8808602E+01	5.126E+01
8-004	Rlrrrrrlrr	lrrrrrlrr	3.9395336E+01	5.337E+01
8-005	Rlrrrrrlrl	lrrrrrlrl	3.9795226E+01	5.493E+01
8-006	Rlrrrrrllr	lrrrrrllr	4.0191753E+01	5.652E+01
8-007	Rlrrrrrlll	lrrrrrlll	4.0548574E+01	5.806E+01
8-008	Rlrrrrlrrr	lrrrrlrrr	4.1018158E+01	5.986E+01
8-009	Rlrrrrlrrl	lrrrrlrrl	4.1322385E+01	6.130E+01
8-010	Rlrrrrlrlr	lrrrrlrlr	4.1617139E+01	6.269E+01
8-011	Rlrrrrlrll	lrrrrlrll	4.1875364E+01	6.399E+01
8-012	Rlrrrrllrr	lrrrrllrr	4.2191696E+01	6.548E+01
8-013	Rlrrrrllrl	lrrrrllrl	4.2438623E+01	6.684E+01
8-014	Rlrrrrlllr	lrrrrlllr	4.2710418E+01	6.840E+01
8-015	Rlrrrrllll	rllll	4.0788829E+01	5.898E+01
8-016	Rlrrrlrrrr	lrrrr	4.0788829E+01	5.898E+01

8-017	Rlrrrlrrrl	lrrrlrrrl	4.3663185E+01	7.273E+01
8-018	Rlrrrlrrlr	lrrrlrrlr	4.3904242E+01	7.436E+01
8-019	Rlrrrlrrll	lrrrlrrll	4.4113118E+01	7.584E+01
8-020	Rlrrrlrlrr	lrrrlrlrr	4.4366435E+01	7.728E+01
8-021	Rlrrrlrlrl	lrrrlrlrl	4.4563090E+01	7.878E+01
8-022	Rlrrrlrllr	lrrrlrllr	4.4775570E+01	8.033E+01
8-023	Rlrrrlrlll	rlll	4.3198042E+01	7.064E+01
8-024	Rlrrrllrrr	lrrr	4.3198042E+01	7.064E+01
8-025	Rlrrrllrrl	lrrrllrrl	4.5479793E+01	8.525E+01
8-026	Rlrrrllrlr	lrrrllrlr	4.5689098E+01	8.717E+01
8-027	Rlrrrllrll	lrrrllrll	4.5882296E+01	8.970E+01
8-028	Rlrrrlllrr	rlllrr	4.6005196E+01	9.095E+01
8-029	Rlrrrlllrl	rlllrl	4.4240808E+01	7.656E+01
8-030	Rlrrrllllr	rllllr	4.2034581E+01	6.473E+01
8-031	Rlrrrlllll	rlllll	3.9115749E+01	5.235E+01
8-032	Rlrrlrrrrr	lrrrrr	3.9115749E+01	5.235E+01
8-033	Rlrrlrrrrl	lrrrrl	4.2034581E+01	6.473E+01
8-034	Rlrrlrrrlr	lrrrlr	4.4240808E+01	7.657E+01
8-035	Rlrrlrrrll	lrrrll	4.6005196E+01	9.097E+01
8-036	Rlrrlrrlrr	lrr	4.7053443E+01	9.650E+01
8-037	Rlrrlrrlrl	lrrlrrlrl	4.8378349E+01	1.057E+02
8-038	Rlrrlrrllr	lrrlrrllr	4.8575486E+01	1.088E+02
8-039	Rlrrlrrlll	rlll	4.3198042E+01	7.064E+01
8-040	Rlrrlrlrrr	lrrr	4.3198042E+01	7.064E+01
8-041	Rlrrlrlrrl	lrrlrlrrl	4.9223448E+01	1.158E+02
8-042	Rlrrlrlrlr	lrrlrlrlr	4.9415660E+01	1.192E+02
8-043	Rlrrlrlrll	rll	4.7053443E+01	9.650E+01
8-044	Rlrrlrllrr	lrr	4.7053443E+01	9.648E+01
8-045	Rlrrlrllrl	rllrl	4.8900976E+01	1.123E+02
8-046	Rlrrlrlllr	rlllr	4.5128887E+01	8.273E+01
8-047	Rlrrlrllll	rllll	4.0788829E+01	5.898E+01
8-048	Rlrrllrrrr	lrrrr	4.0788829E+01	5.898E+01
8-049	Rlrrllrrrl	lrrrl	4.5128887E+01	8.272E+01
8-050	Rlrrllrrlr	lrrlr	4.8900976E+01	1.123E+02
8-051	Rlrrllrrll	rll	4.7053443E+01	9.648E+01
8-052	Rlrrllrlrr	lrr	4.7053443E+01	9.650E+01
8-053	Rlrrllrlrl	rllrlrl	4.9320171E+01	1.175E+02
8-054	Rlrrllrllr	rllrllr	4.8476611E+01	1.072E+02
8-055	Rlrrllrlll	rlll	4.3198042E+01	7.064E+01
8-056	Rlrrlllrrr	lrrr	4.3198042E+01	7.064E+01
8-057	Rlrrlllrrl	rlllrrl	4.5585034E+01	8.619E+01
8-058	Rlrrlllrlr	rlllrlr	4.4668849E+01	7.953E+01

8-059	Rlrrlllrll	rlllrll	4.3786551E+01	7.358E+01
8-060	Rlrrllllrr	rllllrr	4.2573041E+01	6.758E+01
8-061	Rlrrllllrl	rllllrl	4.1472638E+01	6.200E+01
8-062	Rlrrllllll	rllllll	3.9996627E+01	5.573E+01
8-063	Rlrrlllllll	rlllllll	3.7875935E+01	4.807E+01
8-064	Rlrlrrrrrr	lrrrrrr	3.7875935E+01	4.807E+01
8-065	Rlrlrrrrrl	lrrrrrl	3.9996627E+01	5.573E+01
8-066	Rlrlrrrrlr	lrrrrlr	4.1472638E+01	6.200E+01
8-067	Rlrlrrrrll	lrrrrll	4.2573041E+01	6.758E+01
8-068	Rlrlrrrlrr	lrrrlrr	4.3786551E+01	7.359E+01
8-069	Rlrlrrrlrl	lrrrlrl	4.4668849E+01	7.954E+01
8-070	Rlrlrrrllr	lrrrllr	4.5585034E+01	8.620E+01
8-071	Rlrlrrrlll	rlll	4.3198042E+01	7.064E+01
8-072	Rlrlrrlrrr	lrrr	4.3198042E+01	7.064E+01
8-073	Rlrlrrlrrl	lrrlrrl	4.8476611E+01	1.072E+02
8-074	Rlrlrrlrlr	lrrlrlr	4.9320171E+01	1.176E+02
8-075	Rlrlrrlrll	rll	4.7053443E+01	9.650E+01
8-076	Rlrlrrllrr	lrr	4.7053443E+01	9.648E+01
8-077	Rlrlrrllrl	rllrl	4.8900976E+01	1.123E+02
8-078	Rlrlrrllll	rllll	4.5128887E+01	8.272E+01
8-079	Rlrlrrllll	rllll	4.0788829E+01	5.898E+01
8-080	Rlrlrlrrrr	lrrrr	4.0788829E+01	5.898E+01
8-081	Rlrlrlrrrl	lrrrl	4.5128887E+01	8.273E+01
8-082	Rlrlrlrrlr	lrrlr	4.8900976E+01	1.123E+02
8-083	Rlrlrlrrll	rll	4.7053443E+01	9.648E+01
8-084	Rlrlrlrlrr	lrr	4.7053443E+01	9.650E+01
8-085	Rlrlrlrllr	rl	5.4645952E+01	1.946E+02
8-086	Rlrlrlrllr	rllr	5.0590467E+01	1.397E+02
8-087	Rlrlrlrlll	rlll	4.3198042E+01	7.064E+01
8-088	Rlrlrllrrr	lrrr	4.3198042E+01	7.064E+01
8-089	Rlrlrllrrl	lrrl	5.0590467E+01	1.395E+02
8-090	Rlrlrllrlr	rllrlr	4.9703500E+01	1.250E+02
8-091	Rlrlrllrll	rll	4.7053443E+01	9.650E+01
8-092	Rlrlrlllrr	rlllrr	4.6005196E+01	9.097E+01
8-093	Rlrlrlllrl	rlllrl	4.4240808E+01	7.657E+01
8-094	Rlrlrllllr	rllllr	4.2034581E+01	6.473E+01
8-095	Rlrlrllllll	rllllll	3.9115749E+01	5.235E+01
8-096	Rlrllrrrrr	lrrrrr	3.9115749E+01	5.235E+01
8-097	Rlrllrrrrl	lrrrrl	4.2034581E+01	6.473E+01
8-098	Rlrllrrrlr	lrrrlr	4.4240808E+01	7.656E+01
8-099	Rlrllrrrll	lrrrll	4.6005196E+01	9.095E+01
8-100	Rlrllrrlrr	lrr	4.7053443E+01	9.650E+01

8-101	Rlrllrrlrl	lrrlrl	4.9703500E+01	1.249E+02
8-102	Rlrllrrllr	rllr	5.0590467E+01	1.395E+02
8-103	Rlrllrrlll	rlll	4.3198042E+01	7.064E+01
8-104	Rlrllrrlrr	lrrr	4.3198042E+01	7.064E+01
8-105	Rlrllrrlr l	rllrlrrl	4.9907384E+01	1.303E+02
8-106	Rlrllrrllr	rllrlrlr	4.9502803E+01	1.214E+02
8-107	Rlrllrrll l	rll	4.7053443E+01	9.650E+01
8-108	Rlrllrllrr	lrr	4.7053443E+01	9.648E+01
8-109	Rlrllrllrl	rllrllrl	4.8288164E+01	1.039E+02
8-110	Rlrllrlllr	rllllr	4.5128887E+01	8.273E+01
8-111	Rlrllrllll	rllll	4.0788829E+01	5.898E+01
8-112	Rlrlllrrrr	lrrrr	4.0788829E+01	5.898E+01
8-113	Rlrlllrrrl	lrrrl	4.5128887E+01	8.272E+01
8-114	Rlrlllrrlr	rlllrrlr	4.5783995E+01	8.825E+01
8-115	Rlrlllrrll	rlllrrll	4.5381239E+01	8.422E+01
8-116	Rlrlllrlrr	rlllrlrr	4.4875194E+01	8.122E+01
8-117	Rlrlllrlrl	rlllrlrl	4.4466583E+01	7.805E+01
8-118	Rlrlllrllr	rlllrllr	4.4008209E+01	7.508E+01
8-119	Rlrlllrlll	rlll	4.3198042E+01	7.064E+01
8-120	Rlrllllrrr	rllllrrr	4.2840715E+01	6.950E+01
8-121	Rlrllllrrl	rllllrrl	4.2317190E+01	6.616E+01
8-122	Rlrllllrlr	rllllrlr	4.1745287E+01	6.332E+01
8-123	Rlrllllrll	rllllrll	4.1178183E+01	6.062E+01
8-124	Rlrllllllrr	rllllllrr	4.0366729E+01	5.726E+01
8-125	Rlrllllllrl	rllllllrl	3.9604078E+01	5.418E+01
8-126	Rlrlllllllr	rlllllllr	3.8536284E+01	5.030E+01
8-127	Rlrllllllll	rllllllll	3.6915667E+01	4.507E+01
8-128	Rllrrrrrrr	lrrrrrrr	3.6915667E+01	4.507E+01
8-129	Rllrrrrrrl	lrrrrrrl	3.8536284E+01	5.030E+01
8-130	Rllrrrrrlr	lrrrrrlr	3.9604078E+01	5.418E+01
8-131	Rllrrrrrll	lrrrrrll	4.0366729E+01	5.726E+01
8-132	Rllrrrrlrr	lrrrrlrr	4.1178183E+01	6.062E+01
8-133	Rllrrrrlrl	lrrrrlrl	4.1745287E+01	6.332E+01
8-134	Rllrrrrllr	lrrrrllr	4.2317190E+01	6.616E+01
8-135	Rllrrrrlll	lrrrrlll	4.2840715E+01	6.950E+01
8-136	Rllrrrlrrr	lrrr	4.3198042E+01	7.064E+01
8-137	Rllrrrlrrl	lrrrlrrl	4.4008209E+01	7.508E+01
8-138	Rllrrrlrlr	lrrrlrlr	4.4466583E+01	7.805E+01
8-139	Rllrrrlrll	lrrrlrll	4.4875194E+01	8.122E+01
8-140	Rllrrrlllrr	lrrrllrr	4.5381239E+01	8.421E+01
8-141	Rllrrrlllrl	lrrrllrl	4.5783995E+01	8.824E+01
8-142	Rllrrrllllr	rllllr	4.5128887E+01	8.272E+01

8-143	Rllrrrllll	rllll	4.0788829E+01	5.898E+01
8-144	Rllrrlrrrr	lrrrr	4.0788829E+01	5.898E+01
8-145	Rllrrlrrrl	lrrrl	4.5128887E+01	8.273E+01
8-146	Rllrrlrrlr	lrrlrrlr	4.8288164E+01	1.039E+02
8-147	Rllrrlrrll	rll	4.7053443E+01	9.648E+01
8-148	Rllrrlrlrr	lrr	4.7053443E+01	9.650E+01
8-149	Rllrrlrlrl	lrrlrlrl	4.9502803E+01	1.213E+02
8-150	Rllrrlrllr	lrrlrllr	4.9907384E+01	1.302E+02
8-151	Rllrrlrlll	rlll	4.3198042E+01	7.064E+01
8-152	Rllrrllrrr	lrrr	4.3198042E+01	7.064E+01
8-153	Rllrrllrrl	lrrl	5.0590467E+01	1.395E+02
8-154	Rllrrllrlr	rllrlr	4.9703500E+01	1.249E+02
8-155	Rllrrllrll	rll	4.7053443E+01	9.650E+01
8-156	Rllrrlllrr	rlllrr	4.6005196E+01	9.095E+01
8-157	Rllrrlllrl	rlllrl	4.4240808E+01	7.656E+01
8-158	Rllrrllllr	rllllr	4.2034581E+01	6.473E+01
8-159	Rllrrlllll	rllllll	3.9115749E+01	5.235E+01
8-160	Rllrlrrrrr	lrrrrr	3.9115749E+01	5.235E+01
8-161	Rllrlrrrrl	lrrrrl	4.2034581E+01	6.473E+01
8-162	Rllrlrrlrr	lrrrlr	4.4240808E+01	7.657E+01
8-163	Rllrlrrlrl	lrrrll	4.6005196E+01	9.097E+01
8-164	Rllrlrrlrr	lrr	4.7053443E+01	9.650E+01
8-165	Rllrlrrlrl	lrrlrl	4.9703500E+01	1.250E+02
8-166	Rllrlrrllr	rllrlrrllr	4.9859773E+01	1.276E+02
8-167	Rllrlrrlll	rlll	4.3198042E+01	7.064E+01
8-168	Rllrlrlrrr	lrrr	4.3198042E+01	7.064E+01
8-169	Rllrlrlrrl	rllrlrlrrl	4.9549049E+01	1.225E+02
8-170	Rllrlrlrlr	rllrlrlrlr	4.9457208E+01	1.203E+02
8-171	Rllrlrlrll	rll	4.7053443E+01	9.650E+01
8-172	Rllrlrllrr	lrr	4.7053443E+01	9.648E+01
8-173	Rllrlrllrl	rllrl	4.8900976E+01	1.123E+02
8-174	Rllrlrlllr	rlllr	4.5128887E+01	8.273E+01
8-175	Rllrlrllll	rllll	4.0788829E+01	5.898E+01
8-176	Rllrllrrrr	lrrrr	4.0788829E+01	5.898E+01
8-177	Rllrllrrrl	lrrrl	4.5128887E+01	8.272E+01
8-178	Rllrllrrlr	rllrllrrlr	4.8619199E+01	1.102E+02
8-179	Rllrllrrll	rll	4.7053443E+01	9.648E+01
8-180	Rllrllrlrr	lrr	4.7053443E+01	9.650E+01
8-181	Rllrllrlrl	rllrllrlrl	4.8335452E+01	1.048E+02
8-182	Rllrllrllr	rllrllrllr	4.8240007E+01	1.029E+02
8-183	Rllrllrlll	rlll	4.3198042E+01	7.064E+01
8-184	Rllrlllrrr	lrrr	4.3198042E+01	7.064E+01

8-185	Rllrlllrrl	rlllrrl	4.5585034E+01	8.620E+01
8-186	Rllrlllrlr	rlllrlr	4.4668849E+01	7.954E+01
8-187	Rllrlllrll	rlllrll	4.3786551E+01	7.359E+01
8-188	Rllrllllrr	rllllrr	4.2573041E+01	6.758E+01
8-189	Rllrllllrl	rllllrl	4.1472638E+01	6.200E+01
8-190	Rllrllllll	rllllll	3.9996627E+01	5.573E+01
8-191	Rllrllllll	rllllll	3.7875935E+01	4.807E+01
8-192	Rlllrrrrrr	lrrrrrr	3.7875935E+01	4.807E+01
8-193	Rlllrrrrrl	lrrrrrl	3.9996627E+01	5.573E+01
8-194	Rlllrrrrlr	lrrrrlr	4.1472638E+01	6.200E+01
8-195	Rlllrrrrll	lrrrrll	4.2573041E+01	6.758E+01
8-196	Rlllrrrlrr	lrrrlrr	4.3786551E+01	7.358E+01
8-197	Rlllrrrlrl	lrrrlrl	4.4668849E+01	7.953E+01
8-198	Rlllrrrllr	lrrrllr	4.5585034E+01	8.619E+01
8-199	Rlllrrrlll	rlll	4.3198042E+01	7.064E+01
8-200	Rlllrrlrrr	lrrr	4.3198042E+01	7.064E+01
8-201	Rlllrrlrrl	rlllrrlrrl	4.5834624E+01	8.885E+01
8-202	Rlllrrlrlr	rlllrrlrlr	4.5734217E+01	8.769E+01
8-203	Rlllrrlrll	rlllrrlrll	4.5642662E+01	8.660E+01
8-204	Rlllrrllrr	rlllrrllrr	4.5527060E+01	8.577E+01
8-205	Rlllrrllrl	rlllrrllrl	4.5433311E+01	8.474E+01
8-206	Rlllrrlllr	rlllr	4.5128887E+01	8.272E+01
8-207	Rlllrrllll	rllll	4.0788829E+01	5.898E+01
8-208	Rlllrlrrrr	lrrrr	4.0788829E+01	5.898E+01
8-209	Rlllrlrrrl	rlllrlrrrl	4.4929693E+01	8.192E+01
8-210	Rlllrlrrlr	rlllrlrrlr	4.4822577E+01	8.075E+01
8-211	Rlllrlrrll	rlllrlrrll	4.4727701E+01	7.990E+01
8-212	Rlllrlrlrr	rlllrlrlrr	4.4610270E+01	7.917E+01
8-213	Rlllrlrlrl	rlllrlrlrl	4.4517247E+01	7.841E+01
8-214	Rlllrlrllr	rlllrlrllr	4.4414996E+01	7.767E+01
8-215	Rlllrlrlll	rlll	4.3198042E+01	7.064E+01
8-216	Rlllrllrrr	lrrr	4.3198042E+01	7.064E+01
8-217	Rlllrllrrl	rlllrllrrl	4.4062616E+01	7.545E+01
8-218	Rlllrllrlr	rlllrllrlr	4.3953988E+01	7.471E+01
8-219	Rlllrllrll	rlllrllrll	4.3852278E+01	7.398E+01
8-220	Rlllrlllrr	rlllrlllrr	4.3719110E+01	7.317E+01
8-221	Rlllrlllrl	rlllrlllrl	4.3607222E+01	7.225E+01
8-222	Rlllrllllr	rllllr	4.2034581E+01	6.473E+01
8-223	Rlllrllllll	rllllll	3.9115749E+01	5.235E+01
8-224	Rllllrrrrr	lrrrrr	3.9115749E+01	5.235E+01
8-225	Rllllrrrrl	lrrrrl	4.2034581E+01	6.473E+01
8-226	Rllllrrrlr	rllllrrrlr	4.2771509E+01	6.884E+01

8-227	Rllllrrrll	rllllrrrll	4.2648619E+01	6.799E+01
8-228	Rllllrrlrr	rllllrrlrr	4.2498340E+01	6.719E+01
8-229	Rllllrrlrl	rllllrrlrl	4.2380900E+01	6.651E+01
8-230	Rllllrrllr	rllllrrllr	4.2252449E+01	6.582E+01
8-231	Rllllrrlll	rllllrrlll	4.2125933E+01	6.509E+01
8-232	Rllllrlrrr	rllllrlrrr	4.1942515E+01	6.437E+01
8-233	Rllllrlrrl	rllllrlrrl	4.1812713E+01	6.366E+01
8-234	Rllllrlrlr	rllllrlrlr	4.1678309E+01	6.299E+01
8-235	Rllllrlrll	rllllrlrll	4.1553298E+01	6.237E+01
8-236	Rllllrllrr	rllllrllrr	4.1390232E+01	6.163E+01
8-237	Rllllrllrl	rllllrllrl	4.1254997E+01	6.098E+01
8-238	Rllllrllll	rllllrllll	4.1097213E+01	6.024E+01
8-239	Rllllrllll	rllll	4.0788829E+01	5.898E+01
8-240	Rllllllrrrr	rllllllrrrr	4.0645580E+01	5.864E+01
8-241	Rllllllrrrl	rllllllrrrl	4.0460316E+01	5.766E+01
8-242	Rllllllrrlr	rllllllrrlr	4.0274867E+01	5.687E+01
8-243	Rllllllrrll	rllllllrrll	4.0105387E+01	5.616E+01
8-244	Rllllllrlrr	rllllllrlrr	3.9885911E+01	5.530E+01
8-245	Rllllllrlrl	rllllllrlrl	3.9705695E+01	5.457E+01
8-246	Rllllllrllr	rllllllrllr	3.9497790E+01	5.377E+01
8-247	Rllllllrlll	rllllllrlll	3.9280785E+01	5.294E+01
8-248	Rlllllllrrr	rlllllllrrr	3.8941527E+01	5.174E+01
8-249	Rlllllllrrl	rlllllllrrl	3.8680279E+01	5.080E+01
8-250	Rlllllllrlr	rlllllllrlr	3.8386885E+01	4.978E+01
8-251	Rlllllllrll	rlllllllrll	3.8087790E+01	4.876E+01
8-252	Rllllllllrr	rllllllllrr	3.7641023E+01	4.732E+01
8-253	Rllllllllrl	rllllllllrl	3.7204862E+01	4.595E+01
8-254	Rlllllllllr	rlllllllllr	3.6562390E+01	4.404E+01
8-255	Rllllllllll	rllllllllll	3.5518339E+01	4.114E+01